Petroleum Science 18 (2021) 1069–1085

Contents lists available at ScienceDirect

Petroleum Science

journal homepage: www.keaipublishing.com/en/journals/petroleum-science

Original Paper

Fluid identification and effective fracture prediction based on frequency-dependent AVOAz inversion for fractured reservoirs

Muhammad Ajaz [a], Fang Ouyang [a], Gui-Hai Wang [b], Shuang-Lian Liu [c], Li-Xin Wang [d], Jian-Guo Zhao [a, *]

[a] State Key Laboratory of Petroleum Resources and Prospecting, Key Laboratory of Geophysical Prospecting of CNPC, China University of Petroleum (Beijing), Beijing, 102249, China
[b] China National Oil & Gas Exploration and Development Corporation, Beijing, 100034, China
[c] Sinopec Research Institute of Petroleum Engineering, Beijing, 100101, China
[d] Sinopec North China E&P Company, Beijing, 100728, China

ARTICLE INFO

Article history:
Received 30 October 2020
Accepted 21 May 2021
Available online 15 July 2021

Edited by Jie Hao

Keywords:
Frequency-dependent AVOAz inversion
P-wave anisotropy
Seismic dispersion
Effective fractures
Fluid identification

ABSTRACT

Fluid and effective fracture identification in reservoirs is a crucial part of reservoir prediction. The frequency-dependent AVO inversion algorithms have proven to be effective for identifying fluid through its dispersion property. However, the conventional frequency-dependent AVO inversion algorithms based on Smith & Gidlow and Aki & Richards approximations do not consider the acquisition azimuth of seismic data and neglect the effect of seismic anisotropic dispersion in the actual medium. The aligned fractures in the subsurface medium induce anisotropy. The seismic anisotropy should be considered while accounting for the seismic dispersion properties through fluid-saturated fractured reservoirs. Anisotropy in such reservoirs is frequency-related due to wave-induced fluid-flow (WIFF) between interconnected fractures and pores. It can be used to identify fluid and effective fractures (fluid-saturated) by using azimuthal seismic data via anisotropic dispersion properties. In this paper, based on Rüger's equation, we derived an analytical expression in the frequency domain for the frequency-dependent AVOAz inversion in terms of fracture orientation, dispersion gradient of isotropic background rock, anisotropic dispersion gradient, and the dispersion at a normal incident angle. The frequency-dependent AVOAz equation utilizes azimuthal seismic data and considers the effect of both isotropic and anisotropic dispersion. Reassigned Gabor Transform (RGT) is used to achieve high-resolution frequency division data. We then propose the frequency-dependent AVOAz inversion method to identify fluid and characterize effective fractures in fractured porous reservoirs. Through application to high-qualified seismic data of dolomite and carbonate reservoirs, the results show that the method is useful for identifying fluid and effective fractures in fluid-saturated fractured rocks.

1. Introduction

It is growing consensuses that the seismic dispersion confines significant information about fluid in the seismic frequency band and could be used as a fluid indicator. Velocity dispersion may be related to the low-frequency shadows, which have been attributed frequently in a substantial number of papers as an effective direct hydrocarbon indicator (Castagna et al., 2003; Chen, 2013; Xiong et al., 2017).

Attempts are commonly made to measure the velocity dispersion in laboratory experiments and some researchers have described the dispersion phenomenon on fluid-saturated rocks (Batzle et al., 2006; Ba et al., 2016; Yin et al., 2017; Ma et al., 2018; Zhao et al., 2019). Winkler and Nur (1979) measured the seismic velocities and attenuation of rocks at different saturation, and partially saturated conditions were observed to be dominant for velocity dispersion. Jones (1986) indicated from the laboratory results that the seismic velocities are the function of frequency at fluid saturation, and the phase-spectrum, frequency-contents, and velocity dispersion can be reliable indicators of the fluid-type present in a reservoir rock. He also inferred that the controlling

* Corresponding author.
E-mail address: zhaojg@cup.edu.cn (J.-G. Zhao).

https://doi.org/10.1016/j.petsci.2021.07.011

factor for the seismic wave dispersion is local viscous flow in porous saturated rocks. Sams et al. (1997) used a collection of VSP, sonic logs, and laboratory measurements on rock samples from a well to detect the elastic properties of fluid-saturated rocks over a broad frequency band. They reported that the fluid in small cracks makes the velocities of the rocks dispersive, accompanying frequency-dependent attenuation at a peak at sonic frequencies. However, the direct comparison between different measurement bands with different resolutions and scales yields non-consistent values. Batzle et al. (2006) documented velocity measurements over the entire frequency range under laboratory conditions to relate dispersion to rocks and fluid properties, and fluid-mobility was quantified as a dominant factor of velocity dispersion at seismic frequencies. However, these dispersion measurements made on rock samples in the laboratory do not consider the effect of fluid-saturated fractures. To the same end, we group has carried out plenty of work relative to low-, medium-, and high-frequency devices development, meanwhile, along with the well-established multi-band facilities for the measurements of rock physical properties, numerical, theoretical and experimental studies on the dispersion of fluid saturated rocks have been conducted (Wang et al., 2012; Zhao et al. 2013, 2015; Sun et al. 2018, 2019; He et al., 2019).

For the past several decades, numerous rock-physics models and theories have been proposed to explain the mechanism producing velocity dispersion. Biot (1962) introduced the generalized theory of seismic wave propagation in fluid-saturated rocks and initially explained the concept of velocity dispersion at macroscopic flow. However, Biot's theory substantially underestimates the measured value of velocity dispersion at seismic frequencies, which could be the result of the squirt-flow mechanism (Dvorkin et al., 1995). White (1975) developed the partial gas saturation model to explain the seismic dispersion in porous rock with mixed fluid saturation at the mesoscopic scale. Dutta and Odé (1979) further revisited this model and coupled it with Biot's theory. Mavko and Nur (1975) introduced the squirt-flow mechanism at microscopic scale due to microcracks in the grains, which was later employed at fully saturated conditions by Dvorkin et al. (1995) to estimate the velocity dispersion due to squirting between interconnected cracks and pores in ultrasonic frequency band. However, in the seismic frequency band Biot-Squirt model has trouble in explaining the seismic velocity dispersion of field data (Pride et al., 2004). At the mesoscopic scale, Berryman and Wang (2000) incorporated fracture-porosity into poroelasticity. They formulated the double-porosity model to analyze the velocity dispersion relation for seismic wave propagation in highly fractured reservoirs. Based on the classic double-porosity theory, Yang et al. (2020) introduced a frequency-dependent elastic model by integrating the squirt-flow effect into Biot's theory, and illustrated the velocity dispersion relation with pore-fluid viscosity. Considering the anisotropy due to mesoscale fracturing into the analysis, Chapman (2003) developed the frequency-dependent anisotropic model to describe the seismic velocity dispersion and wave attenuation at seismic frequencies.

Besides theoretical investigations, considerable efforts have been made to study the characteristics of frequency-dependent reflection coefficient or velocity through AVO modeling to guide the interpretation of frequency anomalies. Chapman et al. (2005, 2006) considered the effect of a dispersive stratum with an elastic overburden at the reflection coefficients through AVO modeling. They demonstrated that the AVO response is frequency-dependent, and fluid-sensitive dispersion is the primary mechanism of mostly observed frequency anomalies in field data. Ren et al. (2009) studied the characteristics of frequency-dependent reflection amplitudes from a patchy-saturated dispersive interface using numerical modeling and investigated the variation of reflection magnitude at different frequencies due to the effect of velocity dispersion. Liu et al. (2011) further studied the characteristics of frequency-dependent AVO and phase of the seismic reflection and found that the reflection amplitude increases at increasing frequency. Zhao et al. (2014) inspected the frequency-dependent reflectivity from the interface between two diffusive-viscous mediums and observed the amplitude and phase of the reflectivity versus incident angle and frequency varies when considerable dispersion occurs in a fluid-saturated medium.

In recent years considerable attention has been paid to develop the dispersion-dependent seismic attributes from field data to detect the oil and gas-bearing reservoirs (Liu et al., 2018; Wang et al., 2019; Ajaz and Sun, 2020; Li et al., 2020; Luo et al., 2020). Odebeatu et al. (2006) employed the spectral decomposition technique to seismic field datasets to observe amplitude variation with frequency and detected gas-bearing reservoirs associated with abnormally high dispersion anomalies. Wu et al. (2010, 2014) combined a spectral decomposition scheme and frequency-dependent AVO to prove the feasibility of inferring fluid-related seismic dispersion from seismic data. They invented a practical inversion approach, which opened the doors to quantify the dispersion-dependent seismic attributes. Shixin et al. (2011) derived the Shuey equation into the frequency domain and incorporated the Morlet wavelet decomposition method to extract the frequency-dependent seismic attributes. They showed the potential of velocity dispersion gradient in hydrocarbon indication. Sun et al. (2012a, 2014) further studied the frequency-dependent AVO methods combined with spectral decomposition techniques to quantify the seismic dispersion response due to different fluids saturation. They provided the evidence through real data applications that the P-wave velocity dispersion related to gas is significantly high, followed by oil and water saturation shows the least dispersion. Li et al. (2016) and Qin et al. (2016) employed the frequency-dependent AVO scheme proposed by Wilson et al. (2009) and extracted seismic dispersion attributes to delineate clastic and carbonate reservoirs. Liu et al. (2019a, 2019b) improved the Wilson's scheme frequency-dependent AVO inversion and presented its application to the prediction of sweet spots of shale gas and tight gas reservoirs. Zong et al. (2016) extended the elastic impedance equation into the frequency domain to estimate the interstratified dispersive elastic parameters and showed the potential of the P- and S-wave velocities dispersion for fluid identification.

The development of frequency-dependent AVO inversion (FAVO) or frequency-dependent seismic attributes has gained increasing attention and showed certain ability in reservoir prediction. The velocity dispersion gradient obtained by FAVO inversion considers the effect of P-wave velocity dispersion induced by pore-fluid, which can be effectively applied for fluid identification in porous media. However, the above proposed FAVO inversion methods are based on isotropic medium assumption, and the influence of the azimuth was not incorporated. The velocity dispersion gradients based on FAVO equations are therefore unable to account for the effect of fluid-induced anisotropic dispersion in fractured rocks. These limitations further cause misleading results in reservoir description and might obscure the interpretation of fluid-saturated fractured reservoirs. The prediction precision for fluid identification in fractured reservoirs required a method to consider the anisotropy of the subsurface. Therefore, the primary focus of this paper is to introduce a method that can identify the fluid-related dispersion in fractured reservoirs.

In fractured reservoirs, seismic amplitude anisotropy has been widely used to characterize subsurface fractures. The medium containing vertical or near-vertical aligned fractures is equivalents to the horizontal transverse isotropic (HTI) medium. The amplitude versus offset/angle and azimuth (AVOAz) inversion based on the

Rüger equation (Rüger 1997, 1998) is commonly used for anisotropy inversion using P-wave seismic data. The Rüger equation describes the P-wave reflectivity in terms of anisotropic parameters for the HTI medium and provides the theoretical basis for characterizing fractured reservoirs. Over the past two decades, numerous studies have been conducted using P-wave amplitude data to predict fractures based on anisotropy via AVOAz inversion (Bachrach et al., 2009; Sun et al., 2011; Chen et al., 2014; Downton and Roure, 2015; Xue et al., 2017; ; Pan et al., 2021). Chapman et al. (2003) demonstrated that the fluid-saturation in fractures strongly changes rock's anisotropic properties due to fluid exchange between fractures and background rock. They argued this change in anisotropy at different saturations depends on frequency. Anisotropic dispersion is the frequency-dependent character of the anisotropy that represents the variations of anisotropy versus frequency. Modeling demonstrates that the anisotropic dispersion is sensitive to the fluid-flow, fluid-saturation, scale-length and density of the fractures (Chapman, 2003; Kong et al., 2013; Chen et al., 2020). Besides, the field-data analysis (Maultzsch et al., 2007; Chapman et al., 2006) indicates that considering seismic dispersion may provide access to fluid-content and fracture-scale information in fractured reservoirs (Chapman, 2009). Therefore, the anisotropic dispersion may be used as a potential indicator of fluid and effective fracture prediction if an inversion technique could be developed to solve anisotropic dispersion using P-wave seismic data.

In this paper, a frequency-dependent amplitude versus offset/angle and azimuth (FAVOAz) inversion is proposed to estimate the azimuthal or anisotropic dispersion properties using the frequency information. The FAVOAz equation is initially derived in terms of isotropic dispersion gradient and anisotropic dispersion gradient by taking derivatives of isotropic and anisotropic terms of the AVOAz equation (Rüger equation) with respect to frequency. Thereafter, the FAVOAz inversion method is suggested to estimate the anisotropic dispersion properties to identify the fluid in saturated fractured reservoirs. Finally, the feasibility of the FAVOAz inversion method is verified through real seismic data. Practical applications in fractured dolomite and carbonate reservoirs demonstrate the potential of the anisotropic dispersion in hydrocarbon indication. Besides, the method is useful to characterize effective fractures.

2. Theory and methods for fluid identification in porous reservoirs

2.1. Frequency-dependent AVO inversion

The frequency-dependent AVO inversion (FAVO) is evolving into a robust seismic exploration method to predict the fluid properties in oil, gas and water-bearing rocks. The FAVO inversion equations are based on AVO approximations of the Zoeppritz equation, which can be obtained by expanding these AVO approximations into the frequency domain. These AVO approximations include Aki & Richards, Smith & Gidlow and Shuey approximations, etc. The Aki & Richards equation is a simple linearized approximation of the Zoeppritz equation, which describes the variations of P-wave reflection amplitude with offset or incidence angle (AVO) for seismic waves passing in subsurface rock. Mathematically it can be expressed as follows (Aki and Richards, 1980).

$$R(\theta) = L(\theta)\frac{\Delta\alpha}{\overline{\alpha}} + M(\theta)\frac{\Delta\beta}{\overline{\beta}} + N(\theta)\frac{\Delta\rho}{\overline{\rho}} \tag{1}$$

where $R(\theta)$, $\overline{\alpha}$, $\overline{\beta}$ and $\overline{\rho}$ is the P-wave reflectivity, average of P-, S-wave velocities and density respectively, across the interface. $\Delta\alpha$, $\Delta\beta$, $\Delta\rho$ denote the difference of P-, S-wave velocities and density, respectively, across the interface. θ is the average of incidence and transmission angles of the P-wave across the interface. $L(\theta)$, $M(\theta)$, $N(\theta)$ are given by the following expressions

$$\begin{aligned} L(\theta) &= \tfrac{1}{2}\left(1 + \tan^2\theta\right) \\ M(\theta) &= -4\frac{\beta^2}{\alpha^2}\sin^2\theta \\ N(\theta) &= \frac{1}{2}\left(1 - 4\frac{\beta^2}{\alpha^2}\sin^2\theta\right) \end{aligned} \tag{2}$$

Since seismic wave propagation in real earth medium experiences velocity dispersion due to WIFF in porous rocks. Thus, assuming, α, β, ρ and $R(\theta)$ are frequency-dependent. Therefore, following the similar procedure of Wilson et al. (2009), frequency information can be introduced in Eq. (1) to express it into frequency-domain as follows

$$R(\theta,f) = L(\theta)\frac{\Delta\alpha}{\overline{\alpha}}(f) + M(\theta)\frac{\Delta\beta}{\overline{\beta}}(f) + N(\theta)\frac{\Delta\rho}{\overline{\rho}}(f) \tag{3}$$

The FAVO inversion equations can be derived by expanding Eq. (3) by Taylor series at a reference frequency (f_0), which can be expressed as follows (Sun et al., 2014).

$$\begin{aligned} R(\theta,f) = {} & L(\theta)\frac{\Delta\alpha}{\overline{\alpha}}(f_0) + (f-f_0)L(\theta)I_X + M(\theta)\frac{\Delta\beta}{\overline{\beta}}(f_0) + (f-f_0)M(\theta)I_Y \\ & + N(\theta)\frac{\Delta\rho}{\overline{\rho}}(f_0) + (f-f_0)N(\theta)I_Z \end{aligned} \tag{4}$$

where f_0 is the dominant frequency and I_X, I_Y, I_Z are the derivatives of P-, S-wave velocities and density with respect to frequency and known as the dispersion gradients of P-, S-wave velocities and density respectively (Sun et al., 2014). The following expressions give these terms.

$$I_X = \frac{d}{df}\left(\frac{\Delta\alpha}{\overline{\alpha}}\right),\ I_Y = \frac{d}{df}\left(\frac{\Delta\beta}{\overline{\beta}}\right),\ I_Z = \frac{d}{df}\left(\frac{\Delta\rho}{\overline{\rho}}\right) \tag{5}$$

The above Eq. (4) is a linear form of FAVO inversion, which can be used to invert the P-wave velocity dispersion gradient term (I_X) from pre-stack seismic data. It is sensitive to the pore-fluid and is often used as a tool for fluid identification in porous rocks.

2.2. FAVO analysis versus azimuths

In order to account the effect of FAVO inversion (dispersion response) as a function of propagation direction (azimuths), seismic gathers of six azimuths are prepared by sorting seismic pre-stack azimuthal CRP data. Then we obtained iso-frequency sections of pre-stack gathers of all azimuths through Reassigned Gabor Transform (RGT) for FAVO inversion. P-wave velocity dispersion gradient (I_X) across each azimuthal CRP gather is obtained by inverting Eq. (4), as indicated in Fig. 1. The results show that the seismic velocity dispersion signature across each azimuthal gather is different and varies with azimuthal direction, as indicated by red ellipses in Fig. 1. It suggests that the P-wave velocity dispersion experiences frequency-dependent anisotropy, associated with WIFF versus azimuthal direction. The brighter (red) color represents higher values (high intensity) of the velocity dispersion gradient (I_X). The intensity of velocity dispersion of the first three azimuthal gathers 0–30°, 30–60°, 60–90° is low, moderate, and high, respectively. The velocity dispersion intensity of the last three

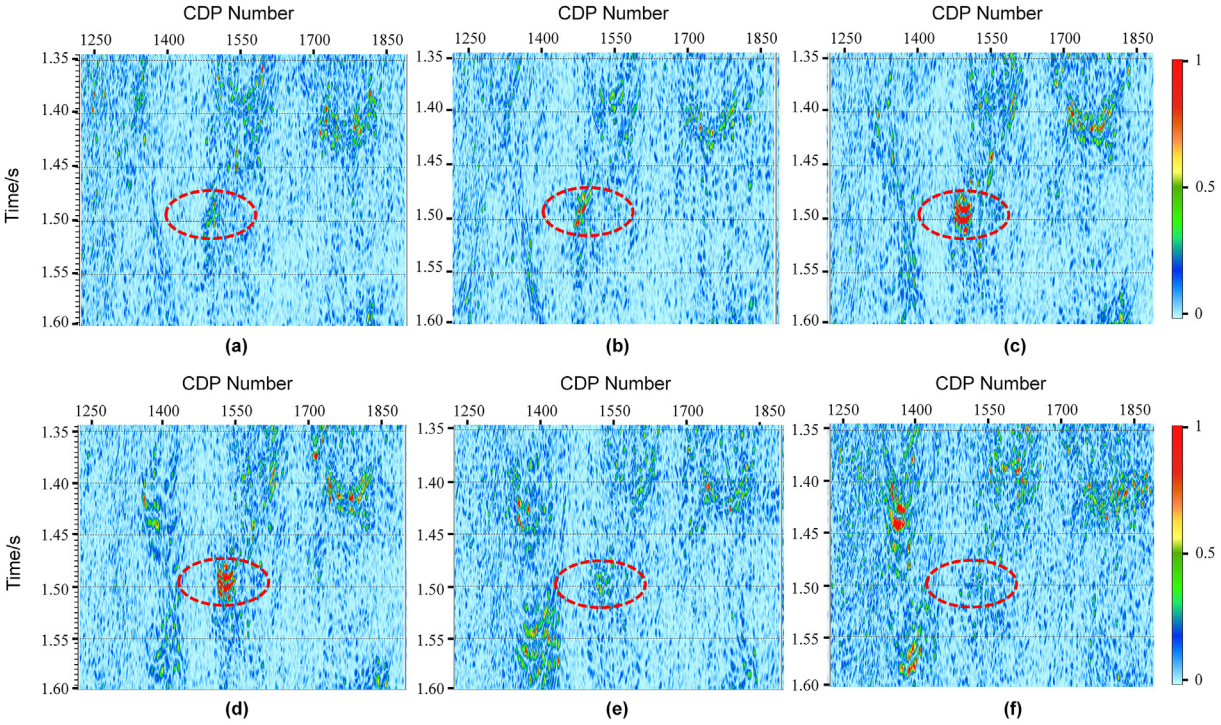

Fig. 1. The inversion results of the P-wave velocity dispersion gradient (I_x) of six azimuthal CRP gathers. (a) 0–30° (b) 30–60° (c) 60–90° (d) 90–120° (e) 120–150° (f) 150–180°. The red ellipses indicate the azimuthal variations of the P-wave velocity dispersion gradient zone. Brighter (red) color represents higher values of the velocity dispersion gradient I_X.

azimuthal gathers 90–120°, 120–150°, 150–180° is high, moderate, and low, respectively. This analysis shows that the azimuth directions of seismic data greatly influence the seismic dispersion, and velocity dispersion shows a dependency on azimuth in anisotropic media. However, the conventional FAVO inversion methods use seismic CRP gathers, which ignore azimuthal information and are limited to the isotropic medium. In principle, the solution of seismic velocity dispersion obtained from conventional FAVO inversion does not account for the effect of anisotropic dispersion. Therefore, it might obscure the interpretation of saturated fractured reservoirs.

The analysis of azimuthally varying FAVO can be used to understand the velocity dispersion response due to WIFF in the direction parallel and perpendicular to the fractures in anisotropic media. Therefore, we used azimuthal information of seismic data in the inversion process and presented a method based on AVOAz theory to rule out the anisotropic dispersion properties of the subsurface medium to characterize fluid-saturated fractured rocks. We first expanded the Rüger equation into the frequency domain and derived a new equation for frequency-dependent AVOAz inversion, which utilizes the seismic data of azimuthal CRP gather.

3. Theory and method for fluid identification in fractured reservoirs

3.1. Azimuthal AVO inversion

The azimuthal AVO inversion (AVOAz) is widely used to characterize fractured reservoirs in exploration seismology. AVOAz inversion is based on the Rüger's equation (Rüger 1997, 1998), which describes the variation of P-wave reflection amplitude versus angle and azimuthal direction for media with HTI symmetry. The Rüger equation for the small incidence angle can be deduced further as follows

$$R(i,\phi) = A + B^{\mathrm{iso}}\sin^2 i + B^{\mathrm{ani}}\cos^2(\phi-\phi_s)\sin^2 i \tag{6}$$

where $R(i,\phi)$ is the P-wave reflection amplitude as a function of incidence and azimuthal angles. The parameters ϕ, ϕ_s and i represent acquisition azimuth (observation direction), symmetry axis direction (fracture orientation), and angle of incident, respectively (see Fig. 2). A is the P-wave reflection amplitude at a normal incidence, B^{iso} and B^{ani} are the isotropic and anisotropic gradients, respectively, which can be expressed as

$$\begin{aligned} A &= \frac{1}{2}\frac{\Delta Z}{\overline{Z}} \\ B^{\mathrm{iso}} &= \frac{1}{2}\left[\frac{\Delta\alpha}{\overline{\alpha}} - \left(\frac{2\overline{\beta}}{\overline{\alpha}}\right)^2\frac{\Delta G}{\overline{G}}\right] \\ B^{\mathrm{ani}} &= \frac{1}{2}\left[\Delta\delta^V + 2\left(\frac{2\overline{\beta}}{\overline{\alpha}}\right)^2\Delta\gamma\right] \end{aligned} \tag{7}$$

where

$$Z = \rho\alpha$$

$$G = \rho\beta^2$$

Here, α, β and ρ represent the isotropic background rock velocities of P-, S-wave and density respectively, whereas δ^v and γ are Thomsen (1986) type anisotropic parameters for media with HTI symmetry. The parameter δ^v describes the P-wave velocity variations with phase angle for near-vertical propagation and γ is the shear-wave splitting parameter, which describes the fractional difference between the fast and slow S-wave velocities. G and Z are the vertical S-wave modulus and P-wave impedance, respectively. The parameters in Eq. (7) are defined as a function of contrast

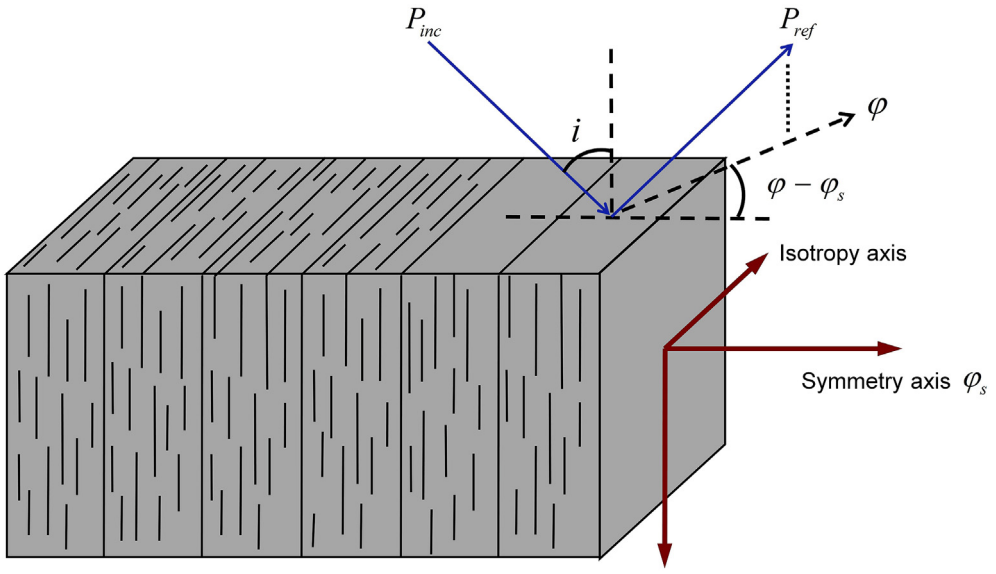

Fig. 2. Sketch of an HTI fracture reservoir model with parallel vertical fractures. P_{inc} and P_{ref} are the incident and reflected P-waves.

across the reflecting boundary. For example, the P-wave velocity contrast in the upper layer (α_1), and the lower layer (α_2) is

$$\frac{\Delta\alpha}{\overline{\alpha}} \text{ with } \overline{\alpha}=\frac{1}{2}(\alpha_1+\alpha_2) \text{ and } \Delta\alpha=\alpha_2-\alpha_1 \tag{8}$$

where the symbols "$\overline{\alpha}$" and "Δ" represent the average and difference of parameters across the reflecting boundary. The azimuthal behavior of $R(i,\phi)$ for unknown symmetry axis (fracture orientation ϕ_s) is related to the anisotropic gradient (B^{ani}) multiplied with the squared cosine of the difference between the acquisition azimuth (ϕ) and the direction of the symmetry axis (ϕ_s). The fracture symmetry (ϕ_s) and anisotropic gradient (B^{ani}) can be obtained by solving Eq. (6) (Al-Marzoug et al., 2006; Sun et al., 2011). The intensity of anisotropic gradient (B^{ani}) represents the degree of fracture development or crack density. Usually, affluent fracture development areas show a strong AVOAz anomaly. Moreover, the parameters γ and δ^{ν} are sensitive to fracture density (Bakulin et al., 2000), and the parameter δ^{ν} is also sensitive to fracture filling.

Rüger Eq. (6) provides the basis for the frequency-dependent AVOAz inversion.

3.2. Derivation of frequency-dependent AVOAz equation

In fluid-saturated rocks, the seismic velocity is frequency-dependent and wave propagation experiences velocity dispersion due to WIFF between interconnected fractures and pores. Studies show that seismic dispersion and fluid saturation have a strong correlation. Especially there may be considerable seismic dispersion in rocks bearing abundant fluid. Therefore, seismic anisotropic dispersion property can be used to identify fluid in fractured reservoirs. Based on Eq. (6), we developed a FAVOAz inversion technique to obtain seismic anisotropic dispersion attribute. The following is the derivation procedure of FAVOAz inversion.

Assuming that $R(i,\phi)$, A , B^{iso} and B^{ani} in Eq. (6) are frequency-dependent. Therefore, Eq. (6) can be express in the frequency-domain as

$$R(i,\phi,f)=A_f+B_f^{\text{iso}}\sin^2 i+B_f^{\text{ani}}\cos^2(\phi-\phi_s)\sin^2 i \tag{9}$$

Expanding Eq. (9) by Taylor series at a reference frequency (f_0) yields the following equation

$$R(i,\phi,f)=A_{f_0}+(f-f_0)\frac{d}{df}A_f+B_{f_0}^{iso}\sin^2 i+(f-f_0)\frac{d}{df}B_f^{\text{iso}}\sin^2 i +B_{f_0}^{\text{ani}}\cos^2(\phi-\phi_s)\sin^2 i+(f-f_0)\frac{d}{df}B_f^{\text{ani}}\cos^2(\phi-\phi_s)\sin^2 i \tag{10}$$

Replacing some terms in Eq. (10) with Eqs. (11)–(13) and further simplification will lead to Eq. (14)

$$R(i,\phi,f_0)=A_{f_0}+B_{f_0}^{\text{iso}}\sin^2 i+B_{f_0}^{\text{ani}}\cos^2(\phi-\phi_s)\sin^2 i \tag{11}$$

$$X_a=\frac{d}{df}A_f,\ X_b=\frac{d}{df}B_f^{\text{iso}},\ X_c=\frac{d}{df}B_f^{\text{ani}} \tag{12}$$

$$\cos^2(\phi-\phi_s)=\frac{1}{2}[1+\cos(2\phi-2\phi_s)] =\frac{1}{2}[1+\cos 2\phi\cos 2\phi_s+\sin 2\phi\sin 2\phi_s] \tag{13}$$

$$R(i,\phi,f)-R(i,\phi,f_0)\approx X_a(f-f_0)+\left(X_b+\frac{1}{2}X_c\right)(f-f_0)\sin^2 i +\frac{1}{2}X_c\cos 2\phi_s(f-f_0)\cos 2\phi\sin^2 i+\frac{1}{2}X_c\sin 2\phi_s(f-f_0)\sin 2\phi\sin^2 i \tag{14}$$

Eq. (14) can be further simplified to obtain Eq. (15) as follows

$$\Delta R(i,\phi,f)\approx C_1(f-f_0)+C_2(f-f_0)\sin^2 i+C_3(f-f_0)\cos 2\phi\sin^2 i +C_4(f-f_0)\sin 2\phi\sin^2 i \tag{15}$$

where

$$\Delta R(i,\phi,f)=R(i,\phi,f)-R(i,\phi,f_0)$$

Eq. (15) is a linear equation in which reference frequency (f_0), series of frequencies $f=(f_1,f_2\ldots\ldots f_N)$, acquisition azimuth (ϕ), and

incident angle (i) are known variables, whereas C_1 C_2, C_3 and C_4 are unknown variables, given by the following expressions

$$\begin{aligned} C_1 &= X_a \\ C_2 &= X_b + \frac{1}{2}X_c \\ C_3 &= \frac{1}{2}X_c \cos 2\phi_s \\ C_4 &= \frac{1}{2}X_c \sin 2\phi_s \end{aligned} \tag{16}$$

The frequencies f_0 and $f = f_1, f_2 \ldots\ldots f_N$ can be obtained from the spectral analysis of seismic data. The selection of f_0 greatly influences the results of FAVOAz inversion. We select the dominant frequency of seismic data as a reference frequency (f_0) since the dispersion response of the seismic data is usually apparent at the dominant frequency. Selecting f_0 at a location where seismic dispersion response is not obvious, the inversion results could be suppressed by noise (Liu et al., 2019b). The above Eq. (15) is named as the FAVOAz equation in this paper, which can be used to invert for the anisotropic dispersion gradient from P-wave pre-stack azimuthal seismic data to identify fluid and characterize effective fractures in fluid-saturated fractured reservoir. The inversion methodology is described in the following section.

3.3. Frequency-dependent AVOAz inversion

The pre-stack seismic amplitude dataset at different azimuth and angle gather in the time domain can be written as a data matrix $R(t, n)$, where t is the sampling interval and n represents traces at each azimuth and angle $(i, \phi) = n$. The time-frequency decomposition can be employed on seismic amplitude dataset $R(t, i, \phi)$ to transform it into spectral amplitudes $S(t, i, \phi, f)$ at the series of frequencies, including reference frequency (f_0), giving a representation

$$R(t, i, \phi) \rightarrow S(t, i, \phi, f) \tag{17}$$

However, spectral amplitudes $S(t, i, \phi, f)$ contain the overprint of the source wavelet (Partyka et al., 1999), which should be removed to recover the actual spectral amplitudes. Wilson et al. (2009) developed a weight function to eliminate the overprint of source wavelets to balance the spectral amplitudes of all frequency components, such that

$$B(t, i, \phi, f) = S(t, i, \phi, f) * W(f, i, \phi) \tag{18}$$

This process is called spectral balancing. Where $B(t, i, \phi, f)$ is the balanced spectral amplitude dataset and $W(f, i, \phi)$ is the weight function for amplitude balancing, which is defined as

$$W(f, i, \phi) = \frac{max(S(f_0, i, \phi))}{max(S(f, i, \phi))} \tag{19}$$

Here, $max(S(f_0, i, \phi))$ is the maximum amplitude at a reference frequency (f_0) and $max(S(f, i, \phi))$ is the maximum amplitude at every single frequency (f). The reference frequency (f_0) is the dominant frequency of pre-stack seismic data. Therefore, incorporating Eqs. (18) and (15) will yield the following equation

$$\begin{aligned} \Delta B(i, \phi, f) \approx\ & C_1(f - f_0) + C_2(f - f_0)\sin^2 i + C_3(f - f_0)\cos 2\phi \sin^2 i \\ & + C_4(f - f_0)\sin 2\phi \sin^2 i \end{aligned} \tag{20}$$

where

$$\Delta B(i, \phi, f) = B(i, \phi, f) - B(i, \phi, f_0)$$

Considering n incident angles and m azimuths of pre-stack CRP gathers, the FAVOAz inversion can be implemented in four steps. First A_{f_0}, $B^{iso}_{f_0}$, $B^{ani}_{f_0}$ can be inverted at reference frequency (f_0) to calculate $B(i_n, \phi_m, f_0)$. The second step is to solve for $\Delta B(i_n, \phi_m, f) = B(i_n, \phi_m, f) - B(i_n, \phi_m, f_0)$ at the series of frequencies $f = f_1, f_2 \ldots\ldots f_N$ by using $B(i_n, \phi_m, f_0)$, whose matrix expression is given by

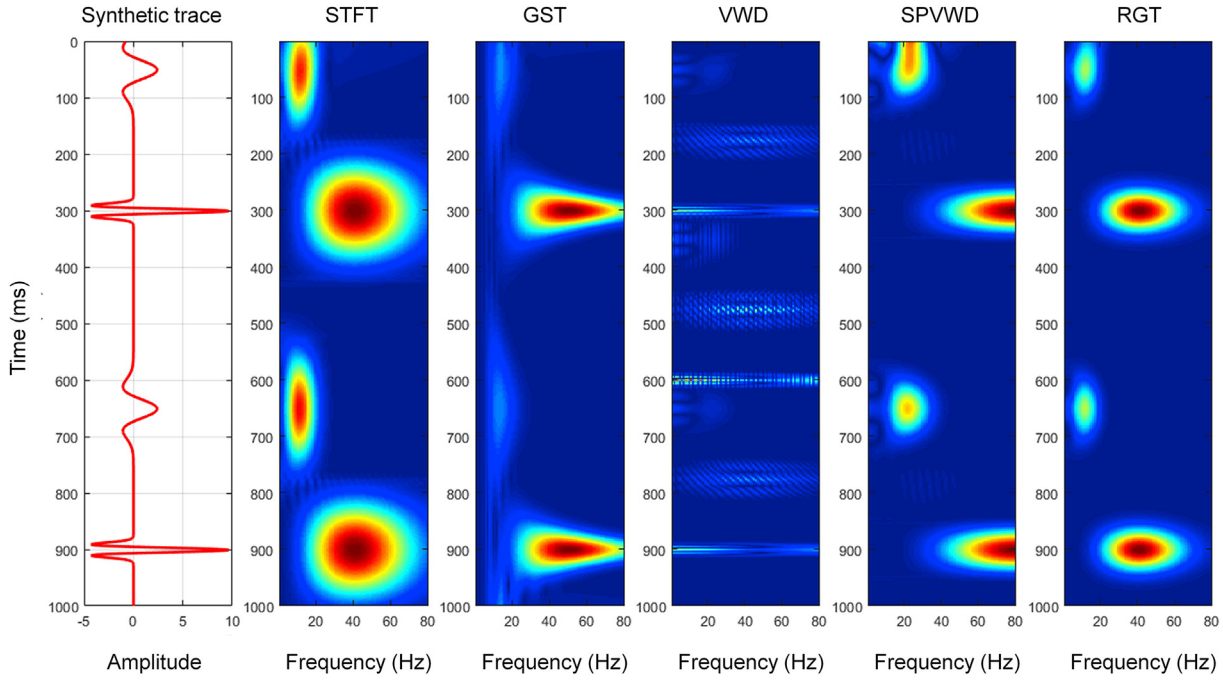

Fig. 3. Time-frequency representation of a synthetic trace via different spectral decomposition techniques of STFT, GST, WVD, SPWVD, RGT. Results indicate that RGT has higher time-frequency resolution, precision and time-frequency localization of signals on the time-frequency plane compared to STFT, GST, WVD, SPWVD.

$$\begin{bmatrix}\Delta B(i_n,\phi_m,f_1)\\ \Delta B(i_n,\phi_m,f_2)\\ \vdots\\ \Delta B(i_n,\phi_m,f_N)\end{bmatrix}=\begin{bmatrix}B(i_n,\phi_m,f_1)\\ B(i_n,\phi_m,f_2)\\ \vdots\\ B(i_n,\phi_m,f_N)\end{bmatrix}-\begin{bmatrix}B(i_n,\phi_m,f_0)\\ B(i_n,\phi_m,f_0)\\ \vdots\\ B(i_n,\phi_m,f_0)\end{bmatrix} \tag{21}$$

where

$n=1,2,...,P;\quad m=1,2...,Q$

Here, P stands for the number of incident angles, and Q stands for the number of azimuths. Thirdly, the unknown C_1, C_2, C_3 and C_4 can be inverted from calculated reflectivity dispersion $\Delta B(i_n,\phi_m,f)$ at a series of frequencies (f) using Eq. (20), whose matrix expression is

$$\begin{bmatrix}\Delta B(i_n,\phi_m,f_1)\\ \Delta B(i_n,\phi_m,f_2)\\ \vdots\\ \Delta B(i_n,\phi_m,f_N)\end{bmatrix}=\begin{bmatrix}(f_1-f_0) & (f_1-f_0)\sin^2 i_n & (f_1-f_0)\cos 2\phi_m\sin^2 i_n & (f_1-f_0)\sin 2\phi_m\sin^2 i_n\\ (f_2-f_0) & (f_2-f_0)\sin^2 i_n & (f_2-f_0)\cos 2\phi_m\sin^2 i_n & (f_2-f_0)\sin 2\phi_m\sin^2 i_n\\ \vdots & \vdots & \vdots & \vdots\\ (f_N-f_0) & (f_N-f_0)\sin^2 i_n & (f_N-f_0)\cos 2\phi_m\sin^2 i_n & (f_N-f_0)\sin 2\phi_m\sin^2 i_n\end{bmatrix}\begin{bmatrix}C_1\\ C_2\\ C_3\\ C_4\end{bmatrix} \tag{22}$$

$$U=VC \tag{23}$$

where

$$U=\begin{bmatrix}\Delta B(i_n,\phi_m,f_1)\\ \Delta B(i_n,\phi_m,f_2)\\ \vdots\\ \Delta B(i_n,\phi_m,f_N)\end{bmatrix},\ V=\begin{bmatrix}(f_1-f_0) & (f_1-f_0)\sin^2 i_n & (f_1-f_0)\cos 2\phi_m\sin^2 i_n & (f_1-f_0)\sin 2\phi_m\sin^2 i_n\\ (f_2-f_0) & (f_2-f_0)\sin^2 i_n & (f_2-f_0)\cos 2\phi_m\sin^2 i_n & (f_2-f_0)\sin 2\phi_m\sin^2 i_n\\ \vdots & \vdots & \vdots & \vdots\\ (f_N-f_0) & (f_N-f_0)\sin^2 i_n & (f_N-f_0)\cos 2\phi_m\sin^2 i_n & (f_N-f_0)\sin 2\phi_m\sin^2 i_n\end{bmatrix}$$

$$C=\begin{bmatrix}C_1\\ C_2\\ C_3\\ C_4\end{bmatrix}$$

Here, C is an unknown column vector containing C_1, C_2, C_3 and C_4. The SVD decomposition method can be applied to Eq. (23) to calculate C. Finally, by using Eq. (16), C_1, C_2, C_3 and C_4 can be used to estimate X_a, X_b, X_c and ϕ_s as follows

$$\begin{aligned}X_a&=C_1,\\ X_b&=C_2-\frac{1}{2}X_c,\\ X_c&=2\sqrt{C_3^2+C_4^2},\\ \phi_s&=\frac{1}{2}\tan^{-1}\frac{C_4}{C_3}\end{aligned} \tag{24}$$

where, X_a is the dispersion gradient of the P-wave reflection amplitude at a normal incidence, and the parameters X_b and X_c are referred to as the isotropic and anisotropic dispersion gradients, respectively. The isotropic gradient term $\left(B^{\text{iso}}\right)$ is dominated by P- and S-waves velocities, as shown in Eq. (7). Therefore, the change rate of B^{iso} with respect to frequency is analogous to the variation of P- and S-wave velocities with respect to frequency. Thus, the isotropic dispersion gradient (X_b) represents the dispersion characteristics of P- and S-wave velocities of background rocks. On the other hand, the anisotropic gradient term B^{ani} is dominated by P- and S-wave velocities and Thomsen's style anisotropic parameters (δ^{ν} and γ) as shown in Eq. (7). The parameters δ^{ν} and γ are also the function of P- and S-wave velocities and sensitive to the fracture density and fracture filling. Therefore, the change rate of B^{ani} with respect to frequency is analogous to the variation of P- and S-wave velocities with respect to frequency in anisotropic rock. Thus, the anisotropic dispersion gradient term (X_c) could be used to describe the anisotropic dispersion properties of fractured rocks. It is sensitive to the fluid response in fractures. The regions with strong anisotropic dispersion can be correlated with hydrocarbon saturation. The WIFF within the fractures causes dispersion in the fractured area to distinguish the fluid-saturated fractures from background rock with a strange dispersion anomaly relative to background rock. Therefore, the anisotropic dispersion gradient term (X_c) could be used to predict the fluid in saturated fractured reservoirs.

An important step for FAVOAz inversion is to decompose seismic amplitude data at multiple frequencies. Therefore, a high-resolution spectral decomposition scheme, Reassigned Gabor Transform (RGT), is selected to acquire multiple iso-frequency pre-stack seismic gathers (spectral amplitudes) for the FAVOAz inversion. To evaluate the precision of RGT, we constructed a synthetic trace composed of Ricker wavelets with two center frequencies, 10 Hz (at time 50 ms and 650 ms) and 40 Hz (at time 300 ms and 900 ms). We made a comparison between RGT and other commonly used spectral decomposition techniques, which include short-time Fourier transform (STFT), Generalized S transform (GST), Wigner-Ville distribution (VWD), smoothed pseudo-Wigner-Ville distribution (SPVWD). Through the comparative analysis, it can be seen (Fig. 3) that the precision of the RGT is higher than the other time-frequency decomposition methods.

A Hamming window of 90 ms length is used for STFT computation. The predefined window length limits the temporal resolution at 50 ms and 650 ms and frequency resolution at 300 ms and 900 ms. Compared with the STFT spectrum, the temporal resolution of GST is improved at higher frequency (40 Hz at times 300 ms and 900 ms). However, the frequency resolution is low. In contrast, at a lower frequency (10 Hz at 50 ms and 650 ms), both temporal and frequency resolution have deteriorated. The WVD spectrum shows the false energy distribution at 180 ms, 480 ms, and 780 ms due to

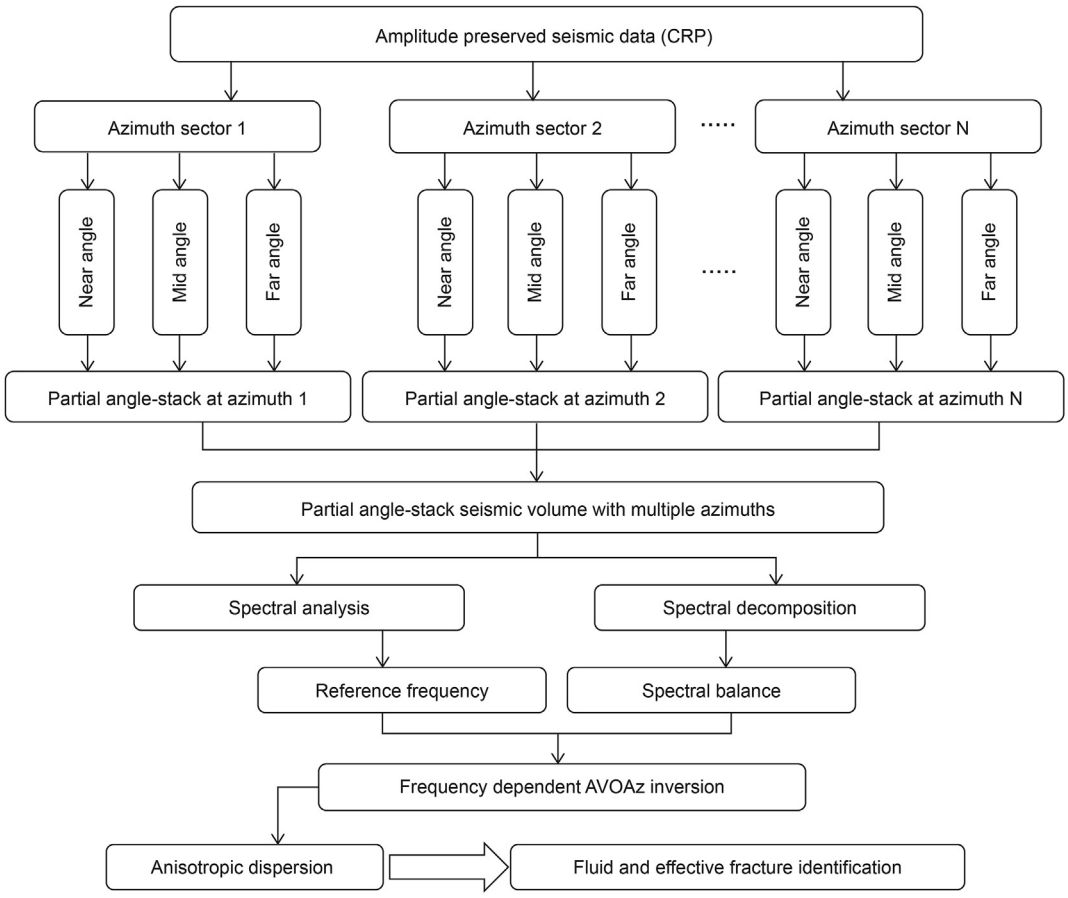

Fig. 4. The workflow of FAVOAz inversion for pre-stack seismic data.

the effect of cross-term interference (CTI). These wrong energy distributions are removed in the SPWVD spectrum. It provides better temporal resolution at both high and low frequencies. However, the frequency resolution is insufficient to reflect the synthetic trace's spectral representation.

The RGT is a modified approach of Gabor transform (GT). It converges the total energy to its center of gravity in the time-frequency plane via a precise energy distribution function. The signals decomposition via RGT has improved the time-frequency representation at lower and higher frequencies. The energy of signals is more concentrated in the time-frequency plane, and both temporal and frequency resolution are improved. In addition, the duration of the RGT spectrum is also close to the period of the wavelet in time. Therefore, Reassigned Gabor Transform (RGT) is used to achieve high-resolution frequency division data for FAVOAz inversion.

4. Applications of frequency-dependent AVOAz inversion

The FAVOAz inversion method integrates both azimuth and frequency data. It can be an effective method to classify fluid-saturated fractured reservoirs. The fluid-induced anomalies, which cannot be identified in the time-domain, will occur in the frequency-domain after the seismic data is transformed into the frequency-domain. Thus, it is applied to the seismic data of the fractured dolomite reservoir of Leijia area, Liaoning Province in China, and the carbonate fracture-cavity reservoir of the Hadexun area, Tarim Basin China, to identify the fluid and effective fractures. Besides, we made integration between the results of FAVOAz inversion (X_c Section), AVOAz inversion (B^{ani} Section), and FAVO inversion (I_X Section) to analyze the efficiency of the FAVOAz inversion method.

4.1. Frequency-dependent AVOAz inversion workflow

The FAVOAz inversion not only requires amplitude preserved azimuthal CRP gathers but also seismic data of relatively high S/N ratio. A workflow of FAVOAz inversion is applied to the seismic field datasets is shown in Fig. 4.

First, pre-stack seismic data is sectored into nine azimuths (0–20°, 20–40°, 40–60°, 60–80°, 80–100°, 100–120°, 120–140°, 140–160°, 160–180°) by sorting amplitude preserved azimuthal CRP data. Subsequently, at each azimuthal sector, three partial angle-stacks (0–11°, 11–22°, 22–33°) are obtained in order to achieve partial angle-stacked seismic volume with multiple azimuths (azimuthal partial angle-stacked gathers). Then, the RGT technique is employed to derive iso-frequency sections from pre-stack amplitude preserved azimuthal partial angle-stacked gathers at multiple frequencies, followed by spectral balancing technique in order to eliminate wavelet overprint. Finally, the P-wave anisotropic dispersion gradient is obtained from pre-stack frequency division azimuthal partial-angle stacked gathers for fluid and effective fracture characterization. In addition, the selection of suitable reference frequency is also important since high frequency corresponds to relatively high temporal resolution. Thus, it is more suitable for FAVOAz inversion.

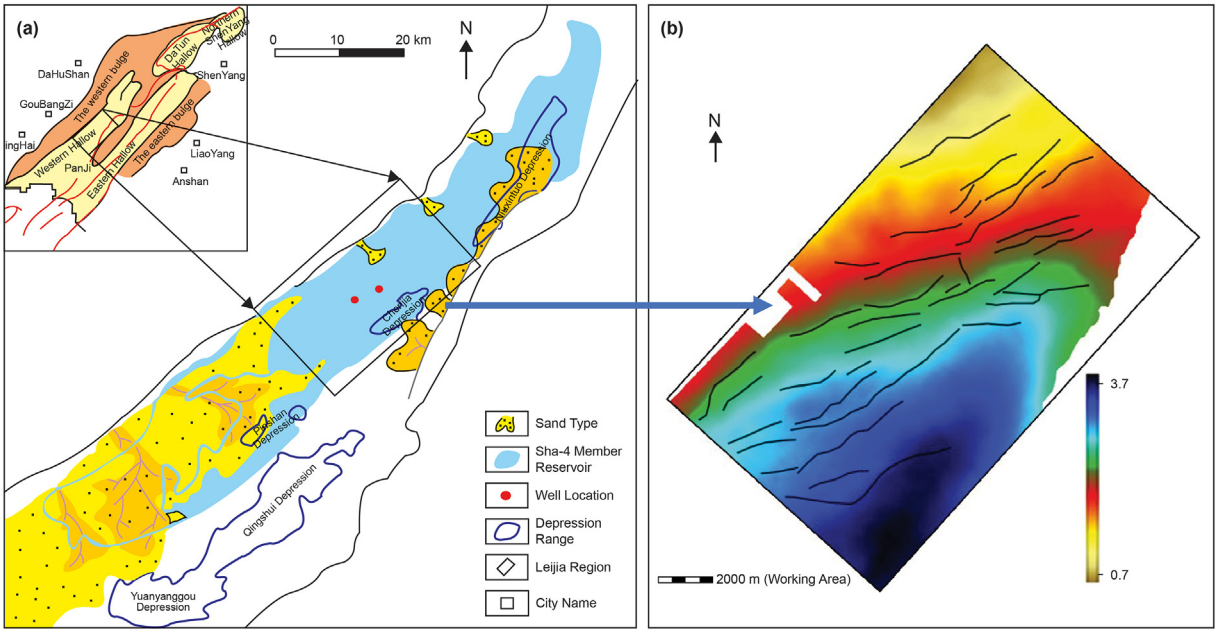

Fig. 5. Map of the Leijia area. (a) The geographic location of Leijia oil field is marked by a black rectangle (b) Time structure map of D3 oil layers. The black lines on the time structure map show faults.

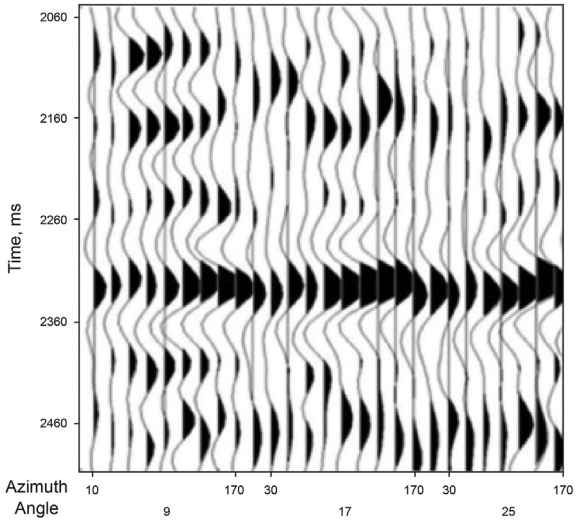

Fig. 6. Partial angle-stacked seismic volume with multiple azimuths showing amplitude azimuthal anisotropy.

4.2. Inversion results analysis of fractured dolomite reservoir

The dolomite reservoirs of Leijia area are located in the north-central part of the Liaohe western depression in Bohai Bay Basin, northeastern China (Fig. 5). The main exploration focus in Leijia area is the dolomites of the Eocene Shahejie Formation (Es4). Es4 is a sedimentary mixing type of typical shallow lacustrine facies, divided into the Gaosheng (GS) and Dujiatai (DJT) oil layers. Research shows that mudstones and thin-bedded dolomites dominate GS formation. These dolomites consist of grained dolomite, mud-bearing dolomite and argillaceous dolomite. The DJT oil layer is further subdivided into D1, D2 and D3 oil layers. Mudstone interbedded with a minor amount of terrigenous clastic rocks is widely distributed in the D1 oil layer. Rocks in the D2 oil layer are composed of mudstone and thin-bedded argillaceous dolomite. The D3 oil layer is one of the main oil-producing layers, primarily consisting of dolomites (argillaceous dolomite and mud-bearing analcite dolomite) interbedded with mudstone and analcite. The important characteristics of the lacustrine dolomite reservoir are (1) High shale and analcite content. (2) Lithology and thickness vary dramatically. (3) Strong heterogeneity. (4) Low porosity and permeability. (5) Complex types of pore structure and diverse storage space.

Reservoir physical properties of the D3 oil layer are affected by sedimentary environment, diagenetic evolution stages, dissolution, mineral composition and tectonic background, etc. The porosity and permeability of the reservoir vary with different lithofacies. The oil content and storage space of dolomites are better than fine-grained mixed rocks (Sun et al., 2012b). The reservoir contains multiple types of storage space. The development of high-quality reservoirs is mainly driven by tectonism and dissolution, while complex dissolution pores and fractures in oil-bearing dolomites primarily control the production of the sweet spot and reservoir output. The high degree fractures development by tectonic activities over various periods formed the main storage space in the dolomite reservoir and usually characterized by strong azimuthal anisotropy at reflection amplitude. The signature of amplitude anisotropy at varying azimuth is shown in Fig. 6. The fractures in the dolomite reservoir are densified by cementation and filling. The fractures filled with mineral cement (calcite and quartz) bring important challenges for producing sweet spots in the dolomite reservoir. Seismic anisotropic signature on reflection amplitude in such reservoirs does not necessarily indicate the productive reservoir. The separation between effective fractures and close fractures is crucial for guiding oil exploration, development, and production in such reservoirs. Therefore, we propose the FAVOAz inversion method to predict effective fracture distribution and fluid in the dolomite reservoir.

The field data of the target reservoir has, significantly high S/N ratio, good lateral continuity, higher vertical resolution and sufficient azimuthal coverage with strong amplitude anisotropy at the reflection azimuths. Before implementing the inversion workflow, the amplitude preserved seismic data with sufficient azimuth

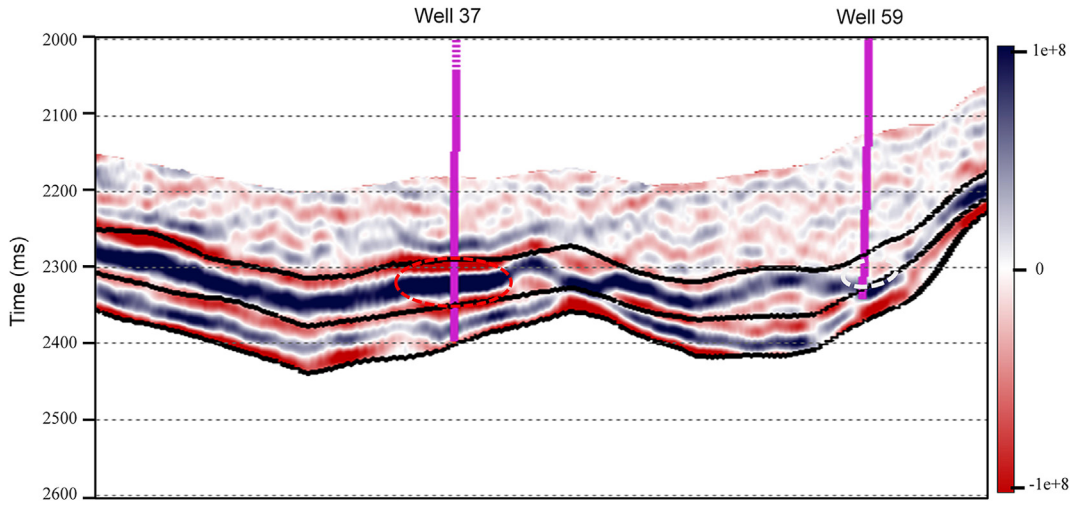

Fig. 7. Seismic post-stack section across oil Well 37 and Well 59.

coverage is required for FAVOAz inversion. In the field data examples, seismic data were preprocessed. The main processing procedures include azimuth sector division, partial angle stacking at each azimuth sector, and sorting partial angle-stacked seismic volume with multiple azimuths, as shown in Fig. 6.

The azimuthal sector division over nine azimuths, ranging from 0° to 180° with 20° interval are 10° (azimuth-range 0°–20°), 30° (azimuth-range 20°–40°), 50° (azimuth-range 40°–60°), 70° (azimuth-range 60°–80°), 90° (azimuth-range 80°–100°), 110° (azimuth-range 100°–120°), 130° (azimuth-range 120°–140°), 150° (azimuth-range 140°–160°), and 170 (azimuth-range 160°–180°). The partial angle-stacked data at each azimuth over three incident angle-range of 0–11°, 11–22°, 22–33° is stacked at 9°, 17°, 25°, respectively (i.e., data assigned to the near angle 9° is stacked over the angle-range 0–11°; data assigned to the mid angle 17° is stacked over the angle-range 11–22°; and data assigned to the far angle 25° is stacked over the angle range 22–33°). Fig. 6 shows the partial angle-stacked seismic volume with multiple azimuths.

We selected a high-productive oil well (Well 37) and a low-productive oil (Well 59) in the Leijia area to analyze inversion results. Fig. 7 shows the seismic post-stack profile through Well 37 and Well 59. Fig. 8 shows the inversion results of FAVOAz, AVOAz, and FAVO through Well 37 and Well 59. The two black lines denote the top and bottom of the D3 member. Fig. 8a shows the inverted results of the anisotropic dispersion gradient (X_c) obtained from the FAVOAz inversion method (by using Eq. (15)). Fig. 8b shows the inverted results of the anisotropic gradient (B^{ani}) obtained from the AVOAz inversion method (by using Eq. (6)). Fig. 8c shows the inversion results of the P-wave velocity dispersion gradient (I_X) obtained from the FAVO inversion method (by using Eq. (4)). In Fig. 9, the predicted results of FAVOAz inversion are compared with the seismic post-stack section and log interpretation, including oil testing results of Well 37. The inversion results of all sections in this paper have been normalized to the range [0–1]. In the following section, we arranged a comparative analysis of X_c, B^{ani}, I_X profiles across Well 37 and Well 59, as shown in Fig. 8.

Fig. 8a shows that the amplitude of anisotropic dispersion gradient (X_c) is strong between the top and bottom of D3 member in the region marked by red dotted ellipse, which indicates that it may be the oil-saturated region. It shows that seismic anisotropic dispersion is sensitive to fluid and reservoir regions with a strong seismic anisotropic dispersion corresponding to hydrocarbon saturation. The drilling test oil results of Well 37 (Fig. 9) show that this region yields a high oil flow of 1.2 tons per day, which validates our prediction based on the anisotropic dispersion gradient (X_c) response in this region. The drilling test oil results indicate that Well 59 does not achieve commercial oil flow in the region marked by a white dotted ellipse, and the anisotropic dispersion gradient (X_c) response is also weak in this region. The comparison of the two wells illustrates that the inversion results of anisotropic dispersion are consistent with the production data. The high-productive oil well is more sensitive to the anisotropic dispersion than the low-productive oil well, as shown in Fig. 8a.

Fig. 8b shows that the anisotropic gradient (B^{ani}) response in the region marked by a red dotted ellipse is strong, which corresponds to the strong anisotropy. The fact that the anisotropy is significant and anisotropic dispersion is strong reflects the region of fracture development containing fluid (effective fractures). The inversion results also match with the drilling test oil results of Well 37 in this region, which further verify our prediction. Both anisotropic intensity and anisotropic dispersion are weak in the region marked by white dotted ellipse at Well 59, which reflects that the sufficient fractures are not developed as well as the oil saturation is not enough to achieve commercial oil flow in this region, which is consistent with production data. Combining X_c with B^{ani} and the oil production data at both wells, we can conclude that the FAVOAz method is useful for effective fracture prediction and fluid identification in anisotropic (fractured) dolomite reservoirs.

The FAVO inversion method has always been a promising method for fluid identification in porous reservoirs. Especially, the gas-bearing reservoir has many successful applications. However, the comparison between Fig. 8a and c shows that the P-wave velocity dispersion gradient (I_X) is relatively weaker than the anisotropic dispersion gradient (X_c) in the reservoir region at oil Well 37. The reason is that the P-wave velocity dispersion gradient (I_X) is computed by the FAVO inversion method, which assumes that the underground reservoir is isotropic. It does not utilize the azimuth of seismic data, ignoring the effect of underground anisotropy. By contrast, the anisotropy is strong in this region, causing the situation that inversion results of I_X do not match with the real condition of the reservoir. Moreover, the difference in I_X response between the high-productive oil region and the low-productive oil region is very small. At the same time, the X_c can be attributed to distinguish the areas of different fluid saturation.

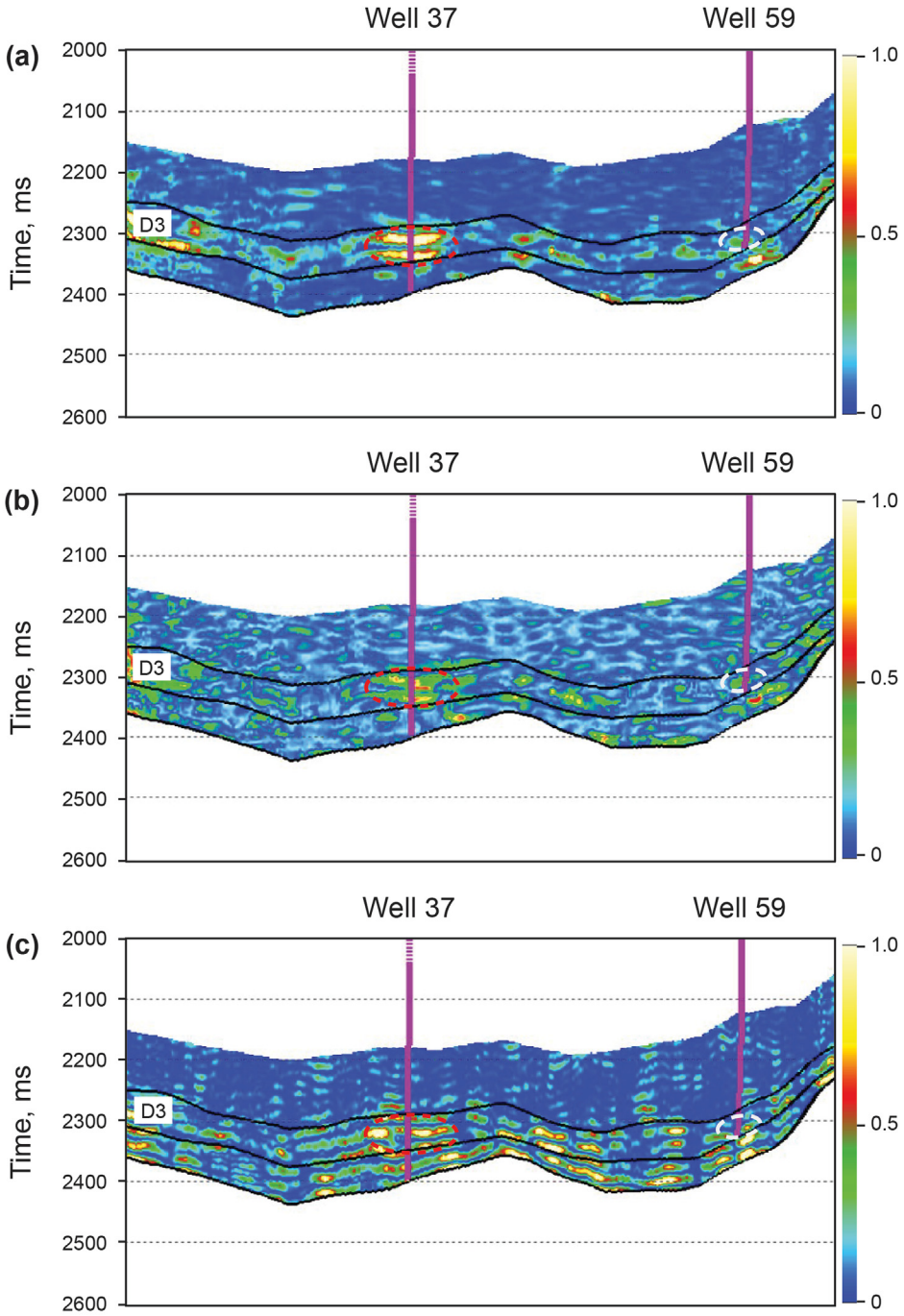

Fig. 8. Comparison between the inversion results of FAVOAz, AVOAz, and FAVO across oil Well 37 and Well 59. (a) Seismic profile of the anisotropic dispersion gradient X_c (b) Seismic profile of the anisotropic gradient B^{ani} (c) Seismic profile of the P-wave velocity dispersion gradient I_X.

The FAVOAz inversion method is based on the Rüger equation, which accounts the effect of subsurface anisotropy in the inversion process by utilizing the azimuth of seismic data. Therefore, the anisotropic dispersion gradient (X_c) calculated from the FAVOAz inversion is more responsive to the real condition of the reservoir. From the above analysis, it can be concluded that the fluid-saturated regions in fractured reservoirs can be characterized by regions correlated with a strong anisotropic dispersion gradient (X_c). The inversion results are also consistent with the production statistics, proving the feasibility of the FAVOAz inversion method.

4.3. Inversion results analysis of fractured carbonate reservoir

The carbonate reservoirs of the Hadexun oil field are located in the north of the Tarim Basin. The tectonic belt is a low-amplitude anticline situated to the south of the Tabei Uplift in the northern Manjiaer Depression (see Fig. 10). The target reservoir is the Ordovician carbonates of the Yijianfang Formation, which contains deeply buried oil, gas, and water reservoirs associated with fracture-cavities. The porosity and permeability of the matrix is quite low due to compaction and diagenetic cementation.

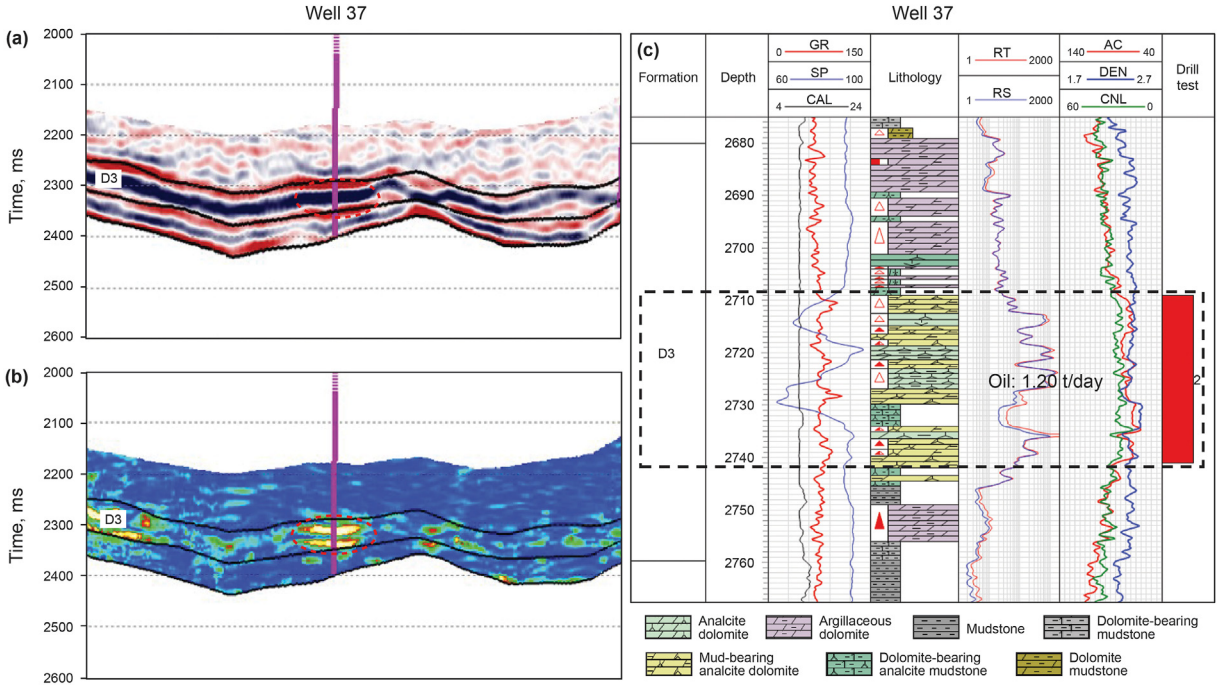

Fig. 9. Comparison between the seismic post-stack profile, FAVOAz inversion profile access high oil productive Well 37 and corresponding interpreted log with oil testing results (a) The seismic post-stack profile (b) Seismic profile of the anisotropic dispersion gradient X_c (c) Log interpretation and oil testing results of Well 37.

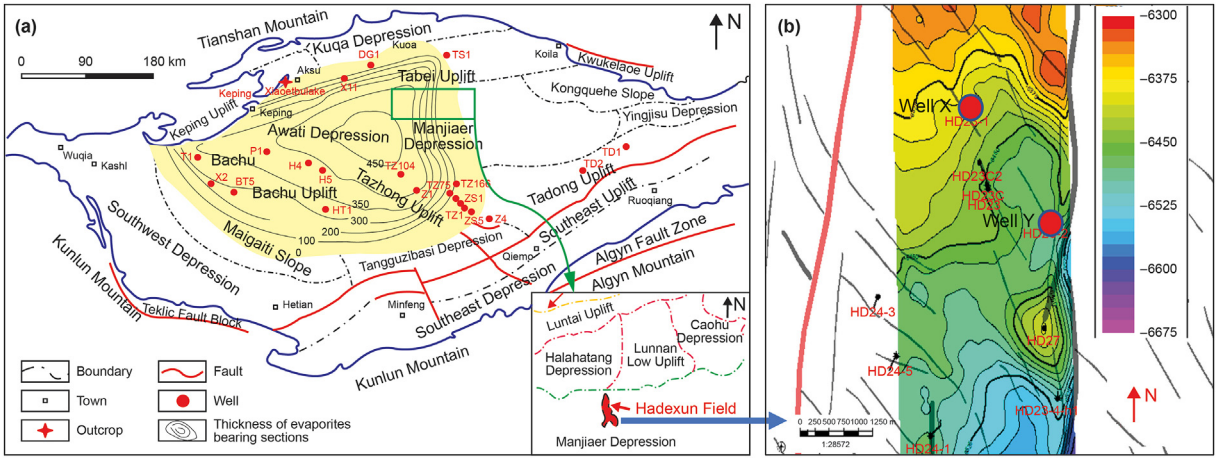

Fig. 10. Map of the Tarim Basin showing the location of the study area (modified from Jiang et al. (2018). (a) Geographic locations of the Hadexun oil field is marked by a black rectangle and corresponding tectonic units are at the bottom of right corner (b) Time structure map of Yijianfang Formation.

Secondary dissolved fracture-cavities provide the dominant storage spaces for fluid accumulation. Fracture-related dissolutions are the primary cause of currently open cavities in the carbonate reservoir (Baqués et al., 2020). These cavities and fractures are influenced by multi-phase tectonic movement, forming complex reservoir distribution associated with the layout of faults and fractures. Detailed characterization of these fracture-cavities is challenging. Therefore, we applied the FAVOAz inversion method to predict fluid in saturated fracture-cavities in this complex reservoir distribution.

We selected two oil wells Well-X and Well-Y, in the carbonate reservoir of the Hadexun area to analyze inversion results. The daily oil production of Well-X and Well-Y is 22.9 tons and 7.9 tons, respectively. The production statistics reveal that Well-X is a high-productive oil well, while the oil-production of Well-Y is low compared to Well-X.

Figs. 11 and 12 show the seismic post-stack profile and inversion results of FAVOAz, AVOAz, and FAVO through Well-X and Well-Y, respectively. Figs. 11a and 12a are the seismic post-stack profiles through Well-X and Well-Y, respectively. Figs. 11b and 12b show the inversion results of the anisotropic dispersion gradient (X_c) through Well-X and Well-Y, respectively, computed from the FAVOAz inversion method (using Eq. (15)). Figs. 11c and 12c show the inversion results of the P-wave anisotropic gradient (B^{ani}) through Well-X and Well-Y, respectively, computed from the AVOAz inversion method (using Eq. (6)). Figs. 11d and 12d show the inversion results of the P-wave velocity dispersion gradient (I_X) across Well-X and Well-Y, respectively, computed from the FAVO inversion method (using Eq. (4)). The following section describes inversion results analysis of X_c, B^{ani}, I_X profiles across Well-X and Well-Y.

Comparing Figs. 11b and 12b, it can be found that in the target

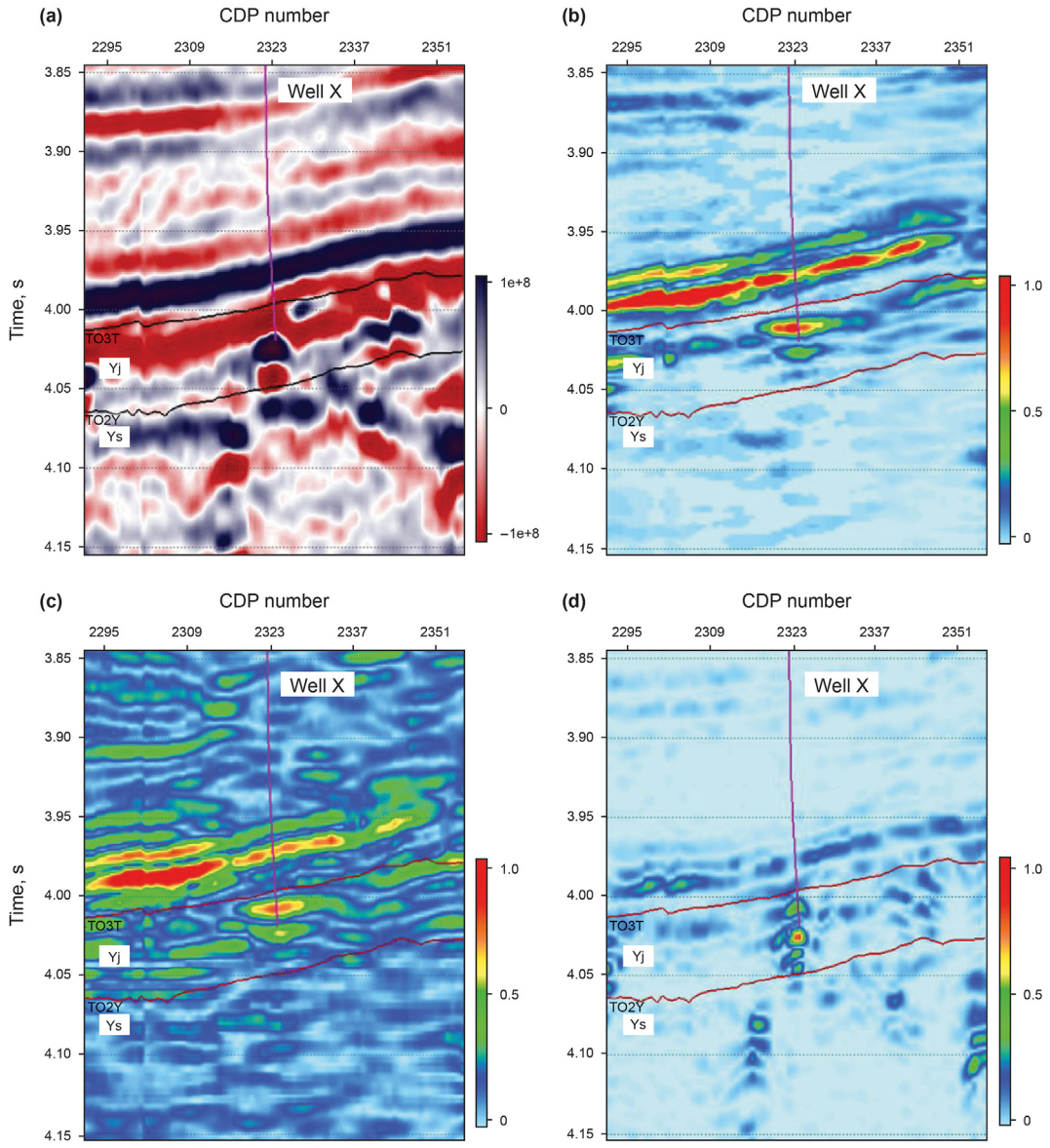

Fig. 11. Comparison between seismic post-stack profile, inversion results of FAVOAz, AVOAz, and FAVO across high-productive oil Well-X (a) Seismic post-stack profile (b) Seismic profile of the anisotropic dispersion gradient X_c (c) Seismic profile of the anisotropic gradient B^{ani} (d) Seismic profile of the P-wave velocity dispersion gradient I_X.

interval, the amplitude of anisotropic dispersion (X_c) across high-productive well (Well-X) is high, while it is weak across low-productive (Well-Y). It is because the X_c is sensitive to the fluid saturation in fractured media and the regions with strong anisotropic dispersion correspond to oil saturation in the target reservoir interval. Our predicted results based on anisotropic dispersion are consistent with the production data, which validates our prediction.

Comparing Figs. 11c and 12c, it can be found that the amplitude of the anisotropic gradient (B^{ani}) across both wells Well-X and Well-Y is strong. However, the lateral response of B^{ani} in the target depth across Well-Y is much stronger than across Well-X. Since the anisotropic gradient (B^{ani}) is related to the azimuthal anisotropy, which may be induced by fractures or stress, while the anisotropic dispersion gradient (X_c) is attributed to the fluid saturation within fractures (effective fractures), therefore, combining B^{ani} and X_c with the oil-production across Well-Y, it can be speculated that the strong anisotropy is caused by stress, and strong anisotropy estimated by B^{ani} corresponding to a limited number of fluid-saturated permeable fractures estimated by X_c to produce oil from low-productive oil Well-Y.

The P-wave velocity dispersion gradient (I_X) reflects the seismic velocity dispersion related to the oil-saturation in cavities in target depth across Well-X and Well-Y. Comparing Figs. 11d and 12d, it can be observed that the I_X profile shows weak amplitude in target depth across Well-X, while it is strong across Well-Y. The low-productive oil well in production depth shows a stronger dispersion anomaly, and the high-productive oil well shows a weak dispersion anomaly, which is not consistent with the well-production data. At the same time, the inversion results of the anisotropic dispersion gradient (X_c) are consistent with the well-production data. It means that fractures provide the permeability to produce oil in the production zone.

Fig. 13 shows the seismic map-view of the inversion results of FAVOAz, AVOAz, and FAVO from the target formation. Fig. 13a shows that the intensity of X_c profile across Well-X is strong and it is weak

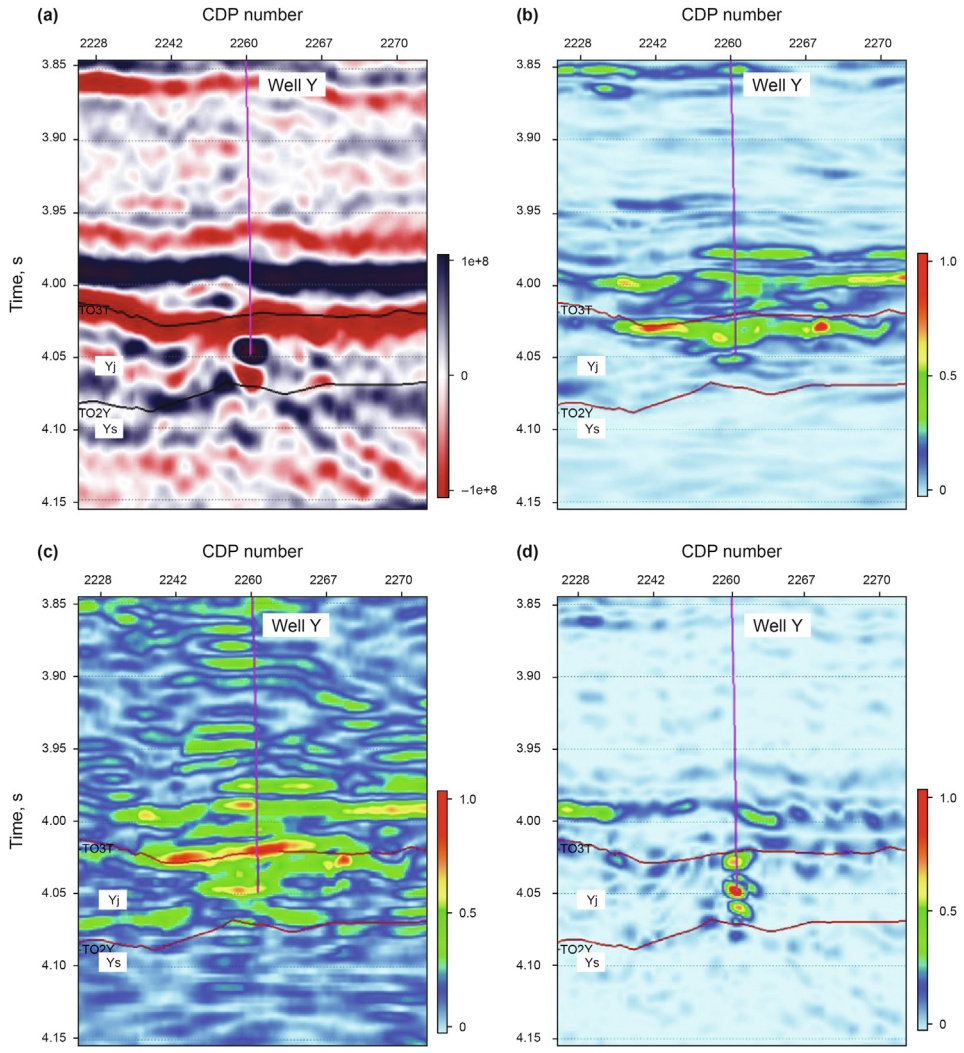

Fig. 12. Comparison between seismic post-stack profile, inversion results of FAVOAz, AVOAz, and FAVO across low-productive oil Well-Y. (a) Seismic post-stack profile (b) Seismic profile of the anisotropic dispersion gradient X_c (c) Seismic profile of the anisotropic gradient B^{ani} (d) Seismic profile of the P-wave velocity dispersion gradient I_X.

across Well-Y, which is consistent with the production data. Moreover, the background energy of the rock is suppressed, and the fracture-cavity reservoir is separated from the background rock, which indicates the seismic anisotropic dispersion related to the oil in the fracture-cavity reservoir. The anisotropic intensity (B^{ani}) across Well-X and Well-Y (Fig. 13b) is relatively stronger than the surrounding rock. However, the lateral response of B^{ani} across Well-Y is much wider than across Well-X. The I_X profile (Fig. 13c) across Well-X and Well-Y reflects the seismic velocity dispersion related to the oil in the production zone, but it does not accurately distinguish the high-productive well from the low-productive well. However, X_c response is more consistent with the actual production statistics and accurately distinguishes the high-productive well from the low-productive well. The above analysis can prove that X_c based on the anisotropic medium is feasible for identifying fluid, and the FAVOAz inversion method is robust for fluid identification in fractured reservoirs.

5. Discussion

The optimization of effective fractures and fluid identification is an important aspect of the productivity of the reservoir. The FAVO inversion and AVOAz inversion are insufficient to estimate the effective fracture distribution and fluid identification in fractured reservoirs. The conventional FAVO inversion, based on the Smith & Gidlow and Aki & Richards approximations, considers the assumptions of isotropic medium and does not take into account the effect of anisotropy of the reservoir rock. AVOAz inversion is based on the Rüger equation, widely used to predict the development of fractures using azimuthal anisotropic intensity. The predicted anisotropic intensity (B^{ani}) of the AVOAz inversion could indicate the reservoir's fracture distribution. However, it does not define effective fractures associated with fluid saturation. Moreover, the directional stress field in the subsurface also induces azimuthal anisotropy, which may cause ambiguity in identifying the fractured zone via anisotropic intensity. Furthermore, the fractures filled with mineral cement (calcite and quartz) bring significant challenges in predicting sweet spots. In such reservoirs, the anisotropic seismic signature does not necessarily indicate the productive reservoir zone.

In this paper, a frequency-dependent amplitude versus offset and azimuth (FAVOAz) inversion method based on the Rüger equation is proposed to estimate the effective fracture distribution and fluid identification in the fractured reservoirs. The formulation of the Rüger equation is based on HTI symmetry, assuming that the parallel vertical fractures are embedded in an isotropic background

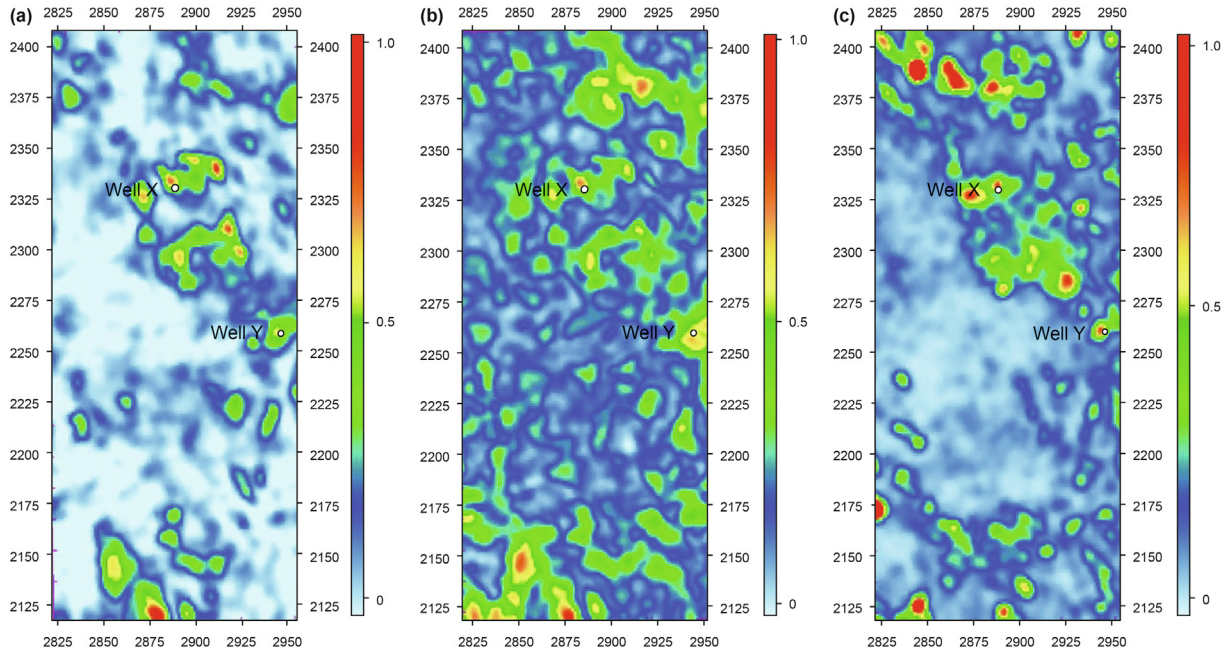

Fig. 13. The seismic map-view of the inversion results of FAVOAz, AVOAz, and FAVO from Yijianfang Formation. (a) Anisotropic dispersion gradient X_c (b) Anisotropic gradient B^{ani} (c) P-wave velocity dispersion gradient I_X.

rock (Rüger, 1998). Introducing frequency information into the Rüger equation ensures that we can reformulate the AVOAz inversion into the frequency domain. The FAVOAz inversion is capable of making full use of the azimuthal amplitude and frequency of seismic data. With this reformulation, the azimuthal dispersion properties of the reservoir can be computed. The predicted intensity of the anisotropic dispersion gradient (X_c) indicates the effective fracture distribution and helpful in identifying fluid in fractured reservoirs. Since the anisotropic dispersion is attributed to the fluid-saturated fractures, it is therefore worthwhile to differentiate fracture-induced anisotropy from stress-induced anisotropy, which will reduce the ambiguity of the interpretation of the reservoir's fracture distribution. We expect that the proposed method will also prove useful in classifying open and close fractures to increase reservoir prediction accuracy. The effective fracture distributions obtained by the FAVOAz inversion will provide further guidance for the oil and gas exploration, development and production.

6. Conclusions

In this paper, we introduced a frequency-dependent AVOAz inversion method to identify fluid and effective fracture based on the AVOAz theory. We extended the Rüger equation in frequency-domain and derived an analytical expression for FAVOAz inversion. The FAVOAz inversion integrates both azimuth and frequency information of seismic data to compute the seismic anisotropic dispersion. The anisotropic dispersion parameter is sensitive to the fluid in fractures, which provides a new attribute for fluid identification and effective fracture prediction in fractured reservoirs. Then, it is applied to the seismic data of the fractured dolomite reservoir of Leijia area, and the carbonate fracture-cavity reservoir of the Hadexun area, in China. The predicted results of FAVOAz inversion are consistent with actual production and logging data, which indicates the reliability of prediction results. Besides, we integrated the results of FAVOAz inversion, AVOAz inversion, and FAVO inversion further to verify the efficiency of the FAVOAz inversion method. The analysis shows that the FAVOAz inversion method is robust for fluid identification and effective fracture prediction in fractured reservoirs and significantly improves reservoir characterization.

Acknowledgments

This work was supported by the National Major Science and Technology Project of China (2016ZX05004003), the National Natural Science Foundation of China (41574103, 41974120, U20B2015), and Open Fund of State Key Laboratory of Coal Resources and Safe Mining (Grant No. SKLCRSM19KFA08).

References

Ajaz, M., Sun, S.Z., 2020. Fluid identification and effective fractures prediction by combining AVOF, AVOZ, and AVOZF inversion in fractured carbonate reservoir. SEG Tech. Progr. Expand. Abstr. 156–160. https://doi.org/10.1190/segam2020-3428075.1.

Aki, K., Richards, P.G., 1980. Quantitative Seismology: Theory and Methods. W. H. Freeman and Co., San Francisco.

Al-Marzoug, A.M., Neves, F.A., Kim, J.J., Nebrija, E.L., 2006. P-wave anisotropy from azimuthal AVO and velocity estimates using 3D seismic data from Saudi Arabia. Geophysics 71 (2), E7–E11. https://doi.org/10.1190/1.2187724.

Ba, J., Zhao, J., Carcione, J.M., Huang, X., 2016. Compressional wave dispersion due to rock matrix stiffening by clay squirt flow: clay Squirt Flow in Tight Siltstone. Geophys. Res. Lett. 43 (12), 6186–6195. https://doi.org/10.1002/2016GL069312.

Bachrach, R., Sengupta, M., Salama, A., Miller, P., 2009. Reconstruction of the layer anisotropic elastic parameters and high-resolution fracture characterization from P-wave data: a case study using seismic inversion and Bayesian rock physics parameter estimation. Geophys. Prospect. 57 (2), 253–262. https://doi.org/10.1111/j.1365-2478.2008.00768.x.

Bakulin, A., Grechka, V., Tsvankin, I., 2000. Estimation of fracture parameters from reflection seismic data—Part I: HTI model due to a single fracture set. Geophysics 65 (6), 1788–1802. https://doi.org/10.1190/1.1444863.

Baqués, V., Ukar, E., Laubach, S.E., Forstner, S.R., Fall, A., 2020. Fracture, dissolution, and cementation events in Ordovician carbonate reservoirs, Tarim Basin, NW China. Geofluids 1–28. https://doi.org/10.1155/2020/9037429.

Batzle, M.L., Han, D.-H., Hofmann, R., 2006. Fluid mobility and frequency-dependent seismic velocity—direct measurements. Geophysics 71 (1). https://doi.org/10.1190/1.2159053. N1–N9.

Berryman, J.G., Wang, H.F., 2000. Elastic wave propagation and attenuation in a double-porosity dual-permeability medium. Int. J. Rock Mech. Min. Sci. 37 (1–2), 63–78. https://doi.org/10.1016/S1365-1609(99)00092-1.

Biot, M.A., 1962. Generalized theory of acoustic propagation in porous dissipative media. J. Acoust. Soc. Am. 34 (9A), 1254–1264. https://doi.org/10.1121/1.1918315.
Castagna, J.P., Sun, S., Siegfried, R.W., 2003. Instantaneous spectral analysis: detection of low-frequency shadows associated with hydrocarbons. Lead. Edge 22 (2), 120–127. https://doi.org/10.1190/1.1559038.
Chapman, M., 2003. Frequency-dependent anisotropy due to meso-scale fractures in the presence of equant porosity. Geophys. Prospect. 51 (5), 369–379. https://doi.org/10.1046/j.1365-2478.2003.00384.x.
Chapman, M., 2009. Modeling the effect of multiple sets of mesoscale fractures in porous rock on frequency-dependent anisotropy. Geophysics 74 (6), D97–D103. https://doi.org/10.1190/1.3204779.
Chapman, M., Liu, E., Li, X.-Y., 2005. The influence of abnormally high reservoir attenuation on the AVO signature. Lead. Edge 24 (11), 1120–1125. https://doi.org/10.1190/1.2135103.
Chapman, M., Liu, E., Li, X.-Y., 2006. The influence of fluid sensitive dispersion and attenuation on AVO analysis. Geophys. J. Int. 167 (1), 89–105. https://doi.org/10.1111/j.1365-246X.2006.02919.x.
Chapman, M., Maultzsch, S., Liu, E., Li, X.-Y., 2003. The effect of fluid saturation in an anisotropic multi-scale equant porosity model. J. Appl. Geophys. 54 (3–4), 191–202. https://doi.org/10.1016/j.jappgeo.2003.01.003.
Chen, H., Li, J., Innanen, K.A., 2020. Inversion of differences in frequency components of azimuthal seismic data for indicators of oil-bearing fractured reservoirs based on an attenuative cracked model. Geophysics 85 (3), R163–R175. https://doi.org/10.1190/geo2019-0152.1.
Chen, H., Zhang, G., Chen, J., Yin, X., 2014. Fracture filling fluids identification using azimuthally elastic impedance based on rock physics. J. Appl. Geophys. 110, 98–105. https://doi.org/10.1016/j.jappgeo.2014.09.006.
Chen, X., 2013. Numerical simulation of frequency-dependent seismic response and gas reservoir delineation in turbidites: a case study from China. J. Appl. Geophys. 94, 22–30. https://doi.org/10.1016/j.jappgeo.2013.04.005.
Downton, J.E., Roure, B., 2015. Interpreting azimuthal Fourier coefficients for anisotropic and fracture parameters. Interpretation 3 (3). https://doi.org/10.1190/INT-2014-0235.1. ST9–27.
Dutta, N., Odé, H., 1979. Attenuation and dispersion of compressional waves in fluid-filled porous rocks with partial gas saturation (White model)—Part II: Results. Geophysics 44 (11), 1789–1805. https://doi.org/10.1190/1.1440939.
Dvorkin, J., Mavko, G., Nur, A., 1995. Squirt flow in fully saturated rocks. Geophysics 60 (1), 97–107. https://doi.org/10.1190/1.1443767.
He, Y.-X., Wu, X., Wang, S., Zhao, J., 2019. Reflection dispersion signatures due to wave-induced pressure diffusion in heterogeneous poroelastic media. Explor. Geophys. 50 (5), 541–553. https://doi.org/10.1080/08123985.2019.1606208.
Jiang, L., Worden, R.H., Cai, C.F., Shen, A., Crowley, S.F., 2018. Diagenesis of an evaporite-related carbonate reservoir in deeply buried Cambrian strata, Tarim Basin, northwest China. AAPG Bull. 102 (1), 77–102. https://doi.org/10.1306/0328171608517048.
Jones, T.D., 1986. Pore fluids and frequency-dependent wave propagation in rocks. Geophysics 51 (10), 1939–1953. https://doi.org/10.1190/1.1442050.
Kong, L., Gurevich, B., Müller, T.M., Wang, Y., Yang, H., 2013. Effect of fracture fill on seismic attenuation and dispersion in fractured porous rocks. Geophys. J. Int. 195 (3), 1679–1688. https://doi.org/10.1093/gji/ggt354.
Li, Y., Li, J., Chen, X., Zhang, J., Zhou, C., Tang, W., 2020. Nonlinear FAVO dispersion quantification based on the analytical solution of the viscoelastic wave equation. Geofluids 1–15. https://doi.org/10.1155/2020/7616045.
Li, Y., Zhang, L., Wang, D., Shi, S., Cui, X., 2016. Hydrocarbon detection for Ordovician carbonate reservoir using amplitude variation with offset and spectral decomposition. Interpretation 4 (3), SN11–30. https://doi.org/10.1190/INT-2015-0135.1.
Liu, J., He, Z., Liu, X., Huo, Z., Guo, P., 2019a. Using frequency-dependent AVO inversion to predict the "sweet spots" of shale gas reservoirs. Mar. Petrol. Geol. 102, 283–291. https://doi.org/10.1016/j.marpetgeo.2018.12.039.
Liu, J., Ning, J., Liu, X., Liu, C., Chen, T., 2019b. An improved scheme of frequency-dependent AVO inversion method and its application for tight gas reservoirs. Geofluids 1–12. https://doi.org/10.1155/2019/3525818.
Liu, L., Cao, S., Wang, L., 2011. Poroelastic analysis of frequency-dependent amplitude-versus-offset variations. Geophysics 76 (3), C31–C40. https://doi.org/10.1190/1.3552702.
Liu, W., Cao, S., Jin, Z., Wang, Z., Chen, Y., 2018. A novel hydrocarbon detection approach via high-resolution frequency-dependent AVO inversion based on variational mode decomposition. IEEE Trans. Geosci. Rem. Sens. 56 (4), 2007–2024. https://doi.org/10.1109/TGRS.2017.2772037.
Luo, X., Chen, X., Sun, L., Zhang, J., Jiang, W., 2020. Optimizing schemes of frequency-dependent AVO inversion for seismic dispersion-based high gas-saturation reservoir quantitative delineation. J. Seismic Explor. 29 (2), 173–199.
Ma, X.-Y., Wang, S.-X., Zhao, J.-G., Yin, H.-J., Zhao, L.-M., 2018. Velocity dispersion and fluid substitution in sandstone under partially saturated conditions. Appl. Geophys. 15 (2), 188–196. https://doi.org/10.1007/s11770-018-0683-8.
Maultzsch, S., Chapman, M., Liu, E., Li, X., 2007. Anisotropic attenuation in VSP data. J. Seismic Explor. 16 (2), 145–158.
Mavko, G., Nur, A., 1975. Melt squirt in the asthenosphere. J. Geophys. Res. 80 (11), 1444–1448. https://doi.org/10.1029/JB080i011p01444.
Odebeatu, E., Zhang, J., Chapman, M., Liu, E., Li, X.-Y., 2006. Application of spectral decomposition to detection of dispersion anomalies associated with gas saturation. Lead. Edge 25 (2), 206–210. https://doi.org/10.1190/1.2172314.
Pan, X., Zhang, D., Zhang, P., 2021. Fracture detection from Azimuth-dependent seismic inversion in joint time–frequency domain. Sci. Rep. 11 (1), 1–15. https://doi.org/10.1038/s41598-020-80021-w.
Partyka, G., Gridley, J., Lopez, J., 1999. Interpretational applications of spectral decomposition in reservoir characterization. Lead. Edge 18 (3), 353–360. https://doi.org/10.1190/1.1438295.
Pride, S.R., Berryman, J.G., Harris, J.M., 2004. Seismic attenuation due to wave-induced flow. J. Geophys. Res. 109 (B1), 1–19. https://doi.org/10.1029/2003JB002639.
Qin, X., Chen, S., Zhang, S., Li, X., Liu, Y., 2016. The application of frequency-dependent AVO inversion in tight reservoirs area. SEG Tech. Progr. Expand. Abstr. 3548–3552. https://doi.org/10.1190/segam2016-13839860.1.
Ren, H., Goloshubin, G., Hilterman, F.J., 2009. Poroelastic analysis of amplitude-versus-frequency variations. Geophysics 74 (6), N41–N48. https://doi.org/10.1190/1.3207863.
Rüger, A., 1997. P-wave reflection coefficients for transversely isotropic models with vertical and horizontal axis of symmetry. Geophysics 62 (3), 713–722. https://doi.org/10.1190/1.1444181.
Rüger, A., 1998. Variation of P-wave reflectivity with offset and azimuth in anisotropic media. Geophysics 63 (3), 935–947. https://doi.org/10.1190/1.1444405.
Sams, M., Neep, J., Worthington, M., King, M., 1997. The measurement of velocity dispersion and frequency-dependent intrinsic attenuation in sedimentary rocks. Geophysics 62 (5), 1456–1464. https://doi.org/10.1190/1.1444249.
Shixin, Z., Xingyao, Y., Guangzhi, Z., 2011. Dispersion-dependent attribute and application in hydrocarbon detection. J. Geophys. Eng. 8 (4), 498–507. https://doi.org/10.1088/1742-2132/8/4/002.
Sun, C., Tang, G., Zhao, J., Zhao, L., Long, T., Li, M., et al., 2019. Three-dimensional numerical modelling of the drained/undrained transition for frequency-dependent elastic moduli and attenuation. Geophys. J. Int. 219 (1), 27–38. https://doi.org/10.1093/gji/ggz284.
Sun, C., Tang, G., Zhao, J., Zhao, L., Wang, S., 2018. An enhanced broad-frequency-band apparatus for dynamic measurement of elastic moduli and Poisson's ratio of rock samples. Rev. Sci. Instrum. 89 (6), 064503. https://doi.org/10.1063/1.5018152.
Sun, S.Z., Jiang, S., Sun, X., Yang, H., Han, J., Li, Y., 2012a. Fluid identification using frequency-dependent AVO inversion in dissolution caved carbonate reservoir. SEG Tech. Progr. Expand. Abstr. https://doi.org/10.1190/segam2012-1017.1, 1–5.
Sun, S.Z., Wang, Z., Yang, H., Xiao, X., Wang, Y., Chen, L., et al., 2011. P-wave fracture prediction algorithm using pre-stack data with limited azimuth distribution: a case study in the TZ45 area, Tarim Basin, China. Petrol. Sci. 8 (4), 422–432. https://doi.org/10.1007/s12182-011-0160-y.
Sun, S.Z., Yin, D., Xiao, X., Li, X., Zhang, J., 2012b. AVOZ inversion using limited azimuthal data on the prediction of fractured dolomite reservoir: a case study in Leijia area, Liaohe western depression. SEG Tech. Progr. Expand. Abstr. https://doi.org/10.1190/segam2012-1171.1, 1–5.
Sun, S.Z., Yue, H., Zhang, Y., Du, T., Hu, L., 2014. An improved frequency-dependent AVO inversion algorithm for fluid detection. SEG Tech. Progr. Expand. Abstr. 543–7. https://doi.org/10.1190/segam2014-1509.1.
Thomsen, L., 1986. Weak elastic anisotropy. Geophysics 51 (10), 1954–1966. https://doi.org/10.1190/1.1442051.
Wang, P., Li, J., Chen, X., Wang, K., Wang, B., 2019. Fluid discrimination based on frequency-dependent AVO inversion with the elastic parameter sensitivity analysis. Geofluids 1–13. https://doi.org/10.1155/2019/8750127.
Wang, S., Zhao, J., Li, Z., Harris, J.M., Quan, Y., 2012. Differential Acoustic Resonance Spectroscopy for the acoustic measurement of small and irregular samples in the low frequency range. J. Geophys. Res. 117 (B6), 1–13. https://doi.org/10.1029/2011JB008808.
White, J., 1975. Computed seismic speeds and attenuation in rocks with partial gas saturation. Geophysics 40 (2), 224–232. https://doi.org/10.1190/1.1440520.
Wilson, A., Chapman, M., Li, X.-Y., 2009. Frequency-dependent AVO inversion. SEG Tech. Progr. Expand. Abstr. 341–345. https://doi.org/10.1190/1.3255572.
Winkler, K., Nur, A., 1979. Pore fluids and seismic attenuation in rocks. Geophys. Res. Lett. 6 (1), 1–4. https://doi.org/10.1029/GL006i001p00001.
Wu, X., Chapman, M., Li, X.-Y., 2014. Estimating seismic dispersion from pre-stack data using frequency-dependent AVO analysis. J. Seismic Explor. 23 (3), 219–239.
Wu, X., Chapman, M., Wilson, A., Li, X.-Y., 2010. Estimating seismic dispersion from pre-stack data using frequency-dependent AVO inversion. SEG Tech. Progr. Expand. Abstr. 425–9. https://doi.org/10.1190/1.3513759.
Xiong, J., Liu, W., He, Z., Chen, X., Zhang, Y., Yu, G., 2017. Fluid identification method and application of pre-stack and post-stack integration based on seismic low-frequency. Pet Res 2 (1), 90–96. https://doi.org/10.1016/j.ptlrs.2017.06.006.
Xue, J., Gu, H., Cai, C., 2017. Model-based amplitude versus offset and azimuth inversion for estimating fracture parameters and fluid content. Geophysics 82 (2). https://doi.org/10.1190/geo2016-0196.1. M1–17.
Yang, Z.-Q., He, T., Zou, C.-C., 2020. A dynamic elastic model for squirt-flow effect and its application on fluid-viscosity-associated velocity dispersion in reservoir sandstones. Geophysics 85 (4), MR201–M212. https://doi.org/10.1190/geo2019-0312.1.
Yin, H., Zhao, J., Tang, G., Zhao, L., Ma, X., Wang, S., 2017. Pressure and fluid effect on frequency-dependent elastic moduli in fully saturated tight sandstone. J. Geophys. Res. 122 (11), 8925–8942. https://doi.org/10.1002/2017JB014244.
Zhao, H., Gao, J., Liu, F., 2014. Frequency-dependent reflection coefficients in diffusive-viscous media. Geophysics 79 (3), T143–T155. https://doi.org/10.1190/geo2013-0038.1.
Zhao, J., Tang, G., Deng, J., Tong, X., Wang, S., 2013. Determination of rock acoustic

properties at low frequency: a differential acoustical resonance spectroscopy device and its estimation technique. Geophys. Res. Lett. 40 (12), 2975–2982. https://doi.org/10.1002/grl.50346.

Zhao, J., Wang, S., Tong, X., Yin, H., Yuan, D., Ma, X., et al., 2015. Differential acoustic resonance spectroscopy: improved theory and application in the low frequency range. Geophys. J. Int. 202 (3), 1775–1791. https://doi.org/10.1093/gji/ggv234.

Zhao, L., Tang, G., Wang, S., Zhao, J., Wang, X., Liu, H., et al., 2019. Laboratory study of oil saturation and oil/water substitution effects on a sandstone's modulus dispersion and attenuation. Explor. Geophys. 50 (3), 324–335. https://doi.org/10.1080/08123985.2019.1610327.

Zong, Z., Yin, X., Wu, G., 2016. Frequency dependent elastic impedance inversion for interstratified dispersive elastic parameters. J. Appl. Geophys. 131, 84–93. https://doi.org/10.1016/j.jappgeo.2016.05.010.